University of Groningen

Bachelor Thesis

An Evaluation of three Dissimilarity Measures for Alpha Trees in Colored Images

Author:
Felix Zailskas *S3918270*
First Supervisor:
Dr. Michael H.F. Wilkinson
Second Supervisor:
Prof. Dr. Kerstin Bunte

August 25, 2022

Abstract

The α-tree algorithm is used for image segmentation by comparing and grouping adjacent pixels in an image based on a dissimilarity measure. This paper expands on previous research by investigating the Manhattan distance, the Euclidean distance, and the cosine dissimilarity as dissimilarity measures for images in the RGB color space. The dissimilarity measures are first tested on synthetic test images and then used to segment four satellite images. For the synthetic images a quantitative comparison is used to predict results on the satellite data. The resulting segmentation images of the satellite data are compared by eye to ground truth segmentation images with different detail levels at multiple α levels. Appropriate α levels were in the range of $[60, 80]$ for the Manhattan distance, $[70, 110]$ for the Euclidean distance, and $[3, 15]$ for the cosine dissimilarity.

Contents

1 Introduction & Motivation **3**

2 State of the Art **4**
2.1 The Chaining Effect . . . 4
2.1.1 Contrast-based α-Trees . . . 4
2.1.2 Odd Gabor Filters . . . 5

3 Methods **5**
3.1 Dissimilarity measures . . . 5
3.2 Edge detection . . . 7

4 Data Set **8**
4.1 Synthetic Test Data . . . 8
4.1.1 Color Pair Selection . . . 8
4.1.2 Resulting Synthetic Images . . . 9
4.2 Real Satellite Data . . . 11

5 Results **13**
5.1 Synthetic Test Data . . . 13
5.1.1 Manhattan Distance . . . 13
5.1.2 Euclidean Distance . . . 16
5.1.3 Cosine Dissimilarity . . . 19
5.2 Satellite Data . . . 22
5.2.1 General Trends . . . 22
5.2.2 Test Image *a* . . . 24
5.2.3 Test Image *b* . . . 27
5.2.4 Test Image *c* . . . 29
5.2.5 Test Image *d* . . . 31

6 Discussion **33**

7 Appendix **36**
7.1 Synthetic Test Images . . . 36
7.2 Synthetic Segmentation Images . . . 42
7.2.1 Manhattan Distance . . . 42
7.2.2 Euclidean Distance . . . 48
7.2.3 Cosine Distance . . . 54

1 Introduction & Motivation

Segmenting certain regions according to predefined criteria is integral to image processing [4]. The analysis of remote images is a practical tool to improve and fasten processes like finding diseases in crops [11], focusing herbicide usage [3], rapid impact assessment for tsunamis, forest fire mapping, earthquake-damage assessment, and landslide extent mapping in disaster management [15] and air- and ocean pollution detection [8, 6]. Images are often represented as a collection of pixels, which do not carry immediate information about connected regions to a computer. Therefore, rules based on the pixel's similarity have to be defined under which the pixels can be connected into humanly understandable areas.
One way of solving this problem is the α-tree algorithm proposed in [7]: Pixels in an image I are grouped into α-connected-components (α-CC) based on some dissimilarity score d between them. Two pixels, $x, y \in I$, belong to the same α-CC if there exists a path of pixels

$$P = \{p_1, p_2, ..., p_i\}$$

where $p_1 = x, p_i = y$, each pair $\{p_k, p_{k+1}\}$ is adjacent and $d(p_k, p_{k+1}) <= \alpha$. Adjacency on a pixel grid is defined as horizontal and vertical neighbors or horizontal, vertical, and diagonal neighbors. Hence, there is a distinction between 4-α-connected-neighborhoods (4-α-CN) and 8-α-connected-neighborhoods (8-α-CN). The α hyper-parameter defines the dissimilarity threshold to group pixels into the same α-CC. Different hierarchical segmentations can be observed for different α values (Figure 1). Generally, higher α levels result in coarser segmentation (larger α-CCs) but also in lower computation times [7]. Thus, for the α-tree algorithm, it is important to address issues that occur when increasing the α levels to improve performance without losing significant information about the image segmentation.

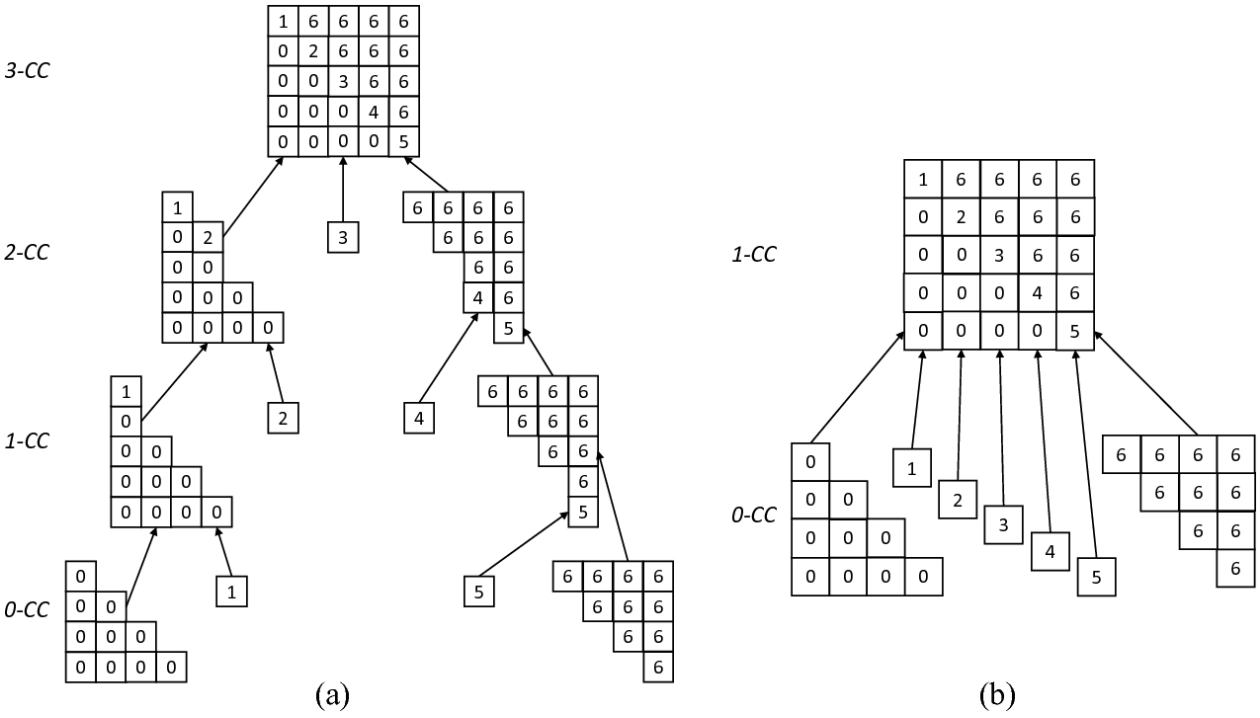

Figure 1: Example of α-trees at different α levels for a 4-α-CN (a) and a 8-α-CN (b). Figure from [17].

Previous research has focused on exploring the α-tree algorithm for gray-scale images. This research will expand on this by investigating three different dissimilarity measures for colored images from the RGB spectrum. These measures will be the Manhattan distance, the Euclidean distance, and the cosine dissimilarity. To improve the performance of the segmentation, we will also use a simple edge detection method. Using these methods, we will answer the research question *"What are appropriate α-levels for the three dissimilarity*

measures, and how well can they be used for detecting relevant sections in colored images?"
The aforementioned sections of agriculture, disaster control, and pollution detection can significantly benefit from this research. Raw satellite image data is often colored; therefore, information is lost when they are converted to gray-scale images for further processing. Furthermore, new avenues of research open up by investigating the α-tree approach for colored images.

2 State of the Art

The α-tree algorithm has been studied well for gray-scale images. The problem of dissimilar regions being connected for low α levels is known as the chaining effect. Previous research showed that using different edge detection techniques can reduce this problem of the α-tree algorithm [13, 17]. In this section, we will first explain the chaining effect in more detail and then present two effective solutions for the chaining effect in gray-scale images.

2.1 The Chaining Effect

Chaining is a major problem for the α-tree algorithm when increasing the α levels. Chaining occurs when two regions with high dissimilarity are connected by a transition region. The transition region is a chain of pixels $C = \{p_1, p_2, ..., p_i\}$ with increasing dissimilarity scores such that $d(p_j, p_{j+1}) \leq \alpha$ while $d(p_1, p_i) > \alpha$ [14]. A gray-scale image with a transition region can be seen in Figure 2. The two very dissimilar regions are sorted into one α-CC even though they represent two different flat zones. There have been multiple proposed solutions for the chaining effect on gray-scale images [12, 13, 14, 17].

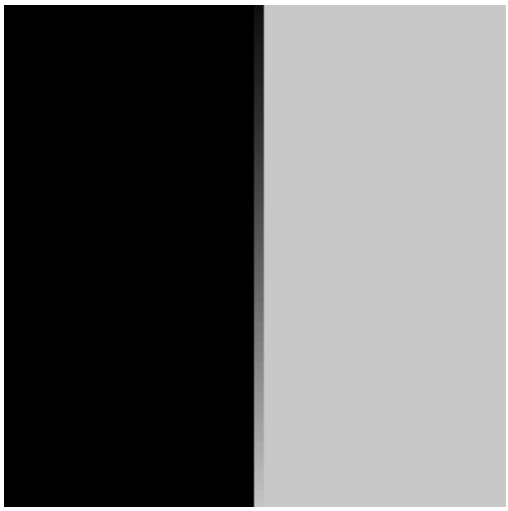

Figure 2: Example of an image that would be subject to the chaining effect. Note the transition region along the y-axis at the center of the x-axis. This image would be classified as one region for lower α levels. Figure from [17].

2.1.1 Contrast-based α-Trees

One way to solve this issue is the contrast-based α-ω-tree based on α-ω-CC [14]. Here, the ω parameter defines the maximal dissimilarity within one α-CC. Although this method reduces the chaining effect, the α-ω-trees only contain a subset of the underlying α-tree's nodes. Due to this reduction of nodes, contrast-based α-trees were proposed in [13]. They work by increasing the dissimilarity along detected edges in the base image. The edges are detected by comparing the absolute difference between pixels at the start and end of a given path. The morphological gradient describes this contrast if the pixel is a transition pixel. Otherwise, the contrast is 0.

2.1.2 Odd Gabor Filters

Another proposed solution is the usage of odd Gabor Filters (GF) which have been shown to perform well in reducing the chaining effect in gray-scale images [17]. The filters detect edges in an image by applying the kernel in a convolution in multiple directions. The kernel can be seen in Figure 3. The angle at which the kernel is applied depends on the α-CN. The directions are $\theta = \{0, \frac{\pi}{2}\}$ for the 4-α-CN and $\theta = \{0, \frac{\pi}{4}, \frac{\pi}{2}, \frac{3\pi}{4}\}$ for the 8-α-CN. The edge detection works best when the GF is applied in parallel to the transition region and worst when applied at a right angle. The improvement in chaining prevention using odd GF was consistent among 4-α-CN and 8-α-CN. While the orientation of the transition region did not seem to impact clean synthetic or noisy images when using odd GF, it did impact the performance on blurry images. Although the odd GF method showed significant improvements for 4-α-CN, it was not performing better than contrast-based α-trees for 8-α-CN when applied to real images.

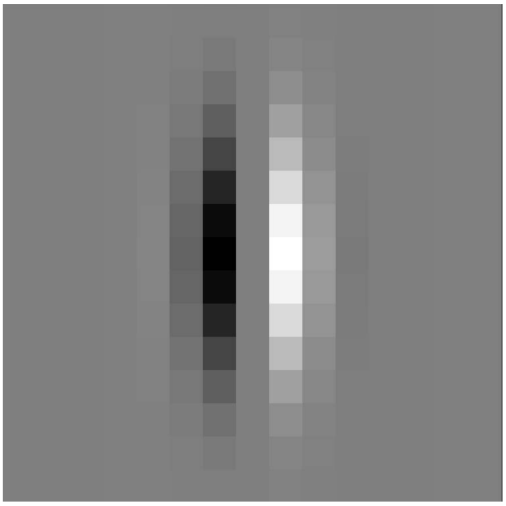

Figure 3: 2D Gabor Filter Kernel. Figure from [17]

3 Methods

This research investigates three different dissimilarity measures for color vectors in the RGB feature space: the Manhattan distance, the Euclidean distance, and the cosine dissimilarity. Other research on α-trees has focused primarily on gray-scale images. However, this approach for image segmentation could also be helpful for colored images. Thus, exploring how the algorithm can be adjusted to be applied to colored images is essential. In this research, the focus will lay on changing the used dissimilarity measure so that it can compare color vectors in the RGB color space. Furthermore, we will examine appropriate α values for the three dissimilarity measures.
RGB color vectors have three components, the red, green, and blue channels. Each channel has a value $x : 0 \leq x \leq 255$ [5]. Different colors can be created based on the three color channels' composition. Figure 4 illustrates the RGB color spectrum.

3.1 Dissimilarity measures

To determine the dissimilarity between two colors, we can treat them as vectors in a 3-dimensional space and use appropriate dissimilarity measures. Based on the results by [2, 9, 10] I have decided to inspect the following three dissimilarity measures. The three dissimilarity measures are visualized in Figure 5.

1. **Manhattan Distance**:
   The Manhattan describes the distance between two points on a grid, measured along the axes at right angles. Let $\vec{x}, \vec{y}$ be two vectors of the same dimension n and elements $x_i, y_i : 0 < i \leq n$, then we can

determine their Manhattan distance by the following equation:

$$D_{\mathrm{M}}(\vec{x}, \vec{y}) = \sum_{i=1}^{n} |x_i - y_i| \tag{1}$$

We see that the vectors are more similar when more of their features are equal. As RGB vectors have 3 dimensions and values in the range $[0, 255]$, we obtain an integer value as the dissimilarity score d for which $0 \leq d \leq 3 * 255$.

2. **Euclidean Distance**:
   The Euclidean distance describes the direct distance between two points. It can also measure dissimilarity between two vectors by treating them as points in the feature space. Let $\vec{x}, \vec{y}$ be two vectors of the same dimension n and elements $x_i, y_i : 0 < i \leq n$, then we can calculate their Euclidean distance with following equation:

$$D_{\mathrm{E}}(\vec{x}, \vec{y}) = \sqrt{\sum_{i=1}^{n} (x_i - y_i)^2} \tag{2}$$

   Similarly to D_{M}, we can see that vectors with a higher difference in their features (color channels) will have a higher D_{E} score. But for this dissimilarity measure, differences are weighted more heavily as they are squared. Note that we obtain a floating point value as the dissimilarity score d for which $0 \leq d \leq \sqrt{3 * 255^2}$.

3. **Cosine Similarity**:
   This measure has been shown to work effectively in information retrieval applications [9, 10]. In information retrieval, feature vectors are created from text documents and compared using the cosine value between the two vectors to obtain a similarity score s. In this paper, we will investigate the effectiveness of this approach for RGB color vectors. As we want to obtain a dissimilarity score, we will define the cosine dissimilarity as $D_{\mathrm{C}} = 1 - |s|$ since the maximum value of the cosine function is 1. The cosine of the angle between two vectors can be calculated using the dot product of the vectors and dividing it by the product of the vectors' lengths [1, 9]. Let $\vec{x}, \vec{y}$ be two vectors of the same dimension n and elements $x_i, y_i : 0 < i \leq n$ with angle θ between them, then:

$$\cos(\theta) = \frac{\vec{x} \cdot \vec{y}}{|\vec{x}||\vec{y}|} \tag{3}$$

   Hence, we can calculate the dissimilarity score D_C using:

$$D_{\mathrm{C}}(\vec{x}, \vec{y}) = 1 - |\cos(\theta)| = 1 - \left| \frac{\vec{x} \cdot \vec{y}}{|\vec{x}||\vec{y}|} \right| \tag{4}$$

   We can see that vectors with similar features (color channels) will have a lower D_{C} score as the cosine value between them will be higher. Note that we obtain a floating point dissimilarity score D_{C} for which $0 \leq d \leq 1$.

As the three similarity measures all produce different ranges of values, their output will be normalized. This will help compare the measures at the same α levels. The output of the similarity measures will be mapped onto the range $[0, 10000]$.

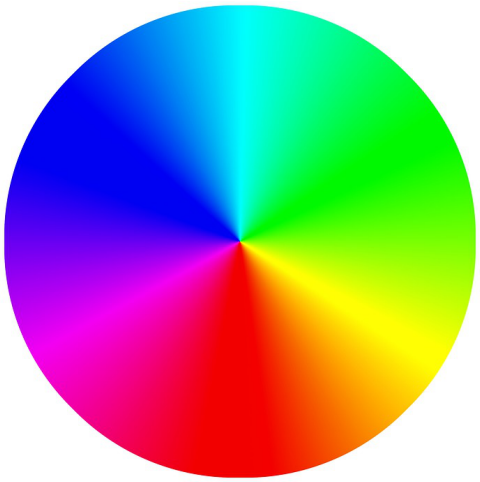

Figure 4: RGB Spectrum visualised on a Color Wheel. Figure from [5]

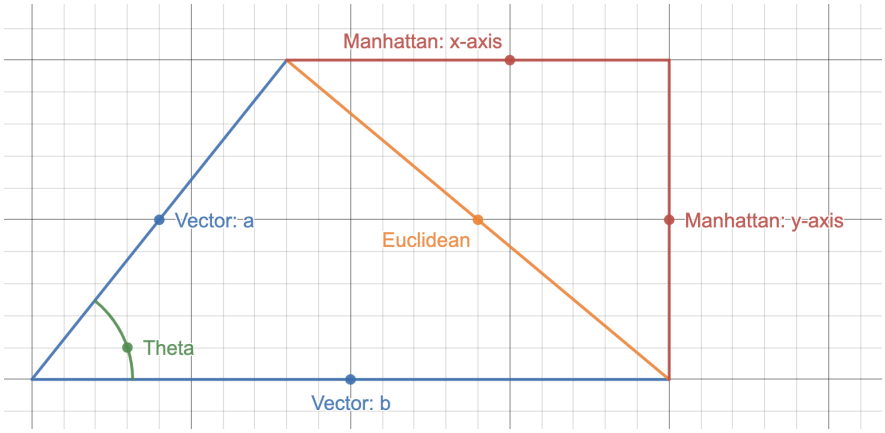

Figure 5: Dissimilarity measures visualised in a 2-dimensional space. D_M is the sum of the red components, normalized. D_E is seen in orange. D_C can be calculated using θ.

3.2 Edge detection

To prevent the chaining effect in our research, we will use a simple method for edge detection. We will investigate the immediate neighborhood for each pixel to determine whether the pixel is on or around an edge. By looking at the dissimilarity scores between the pixel we are currently investigating and its neighbors along a direction, we can strengthen the dissimilarity between the said pixel and its neighbors or leave it the same. This concept can be illustrated with the following example in the 4-α-CN. Take the pixel p_0 at coordinates (x, y). Then we would investigate the dissimilarity between the pixels p_1, p_2 at $(x-1, y)$ and $(x+1, y)$ as well as p_3, p_4 at $(x, y-1)$ and $(x, y+1)$ respectively. We would now increase $d(p_0, p_1)$ and $d(p_0, p_2)$ based on $d(p_1, p_2)$. We assume that $d(p_1, p_2)$ would increase if the chain p_3, p_0, p_4 represents an edge between two regions. Hence, this edge detection increases dissimilarity along edges. This example is visualized in Figure 6. We can see that $d(p_1, p_2)$ is relatively high, while $d(p_3, p_4)$ is relatively low. This would mean the edge detector will increase $d(p_0, p_1)$ and $d(p_0, p_2)$ as it treats the chain p_3, p_0, p_4 as an edge.

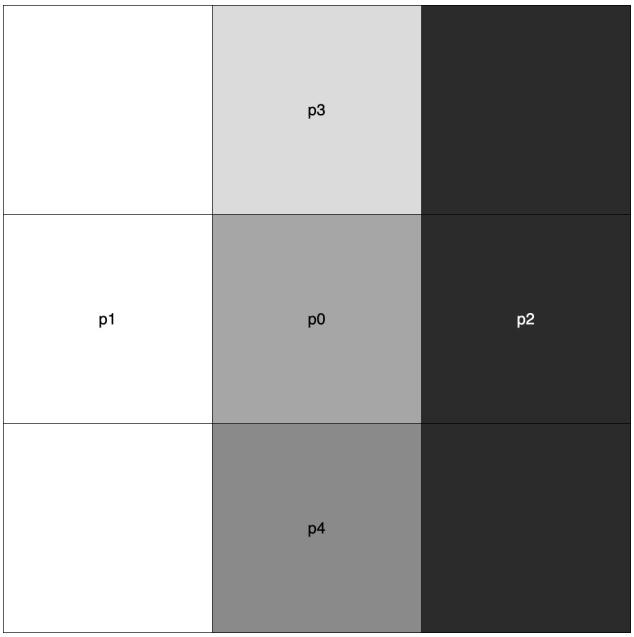

Figure 6: Visualization of the simple edge detector in an 4-α-CN. Here the chain p_3, p_0, p_4 represents an edge between the left and right region.

4 Data Set

This section will describe the data set on which the three dissimilarity measures have been tested. First, we will show how the selection of the synthetic data has been performed. Then we will present the actual satellite data provided for this project.

4.1 Synthetic Test Data

We will first test the different dissimilarity measures on synthetic images. It is essential to decide the colors we will investigate in this preliminary analysis. Theoretically, we can choose between 256^3 colors as each channel has 256 different possible values. Testing this amount of colors is not feasible for this experiment. Hence, we will decide on a subset of colors to test the dissimilarity measures.

4.1.1 Color Pair Selection

By definition, the dissimilarity measures D_{M} and D_{E} do not differentiate between differences in different color channels. We will test this by investigating the segmentation of regions for the color pairs $P_1 = \{(200, 55, 0), (0, 55, 200)\}$ and $P_2 = \{(120, 50, 50), (20, 255, 145)\}$. We see that for these pairs, the sum of the differences in the color channels is the same. Therefore, we assume that $D_{\mathrm{H}}(P_1) = D_{\mathrm{H}}(P_2)$. As D_{E} is based on the square root of the difference in color channels we assume that $D_{\mathrm{E}}(P_1) \approx D_{\mathrm{E}}(P_2)$. The dissimilarity measure D_C does not depend on the difference in color channels.
An interesting property of D_{C} is that two colors that are a multiple of each other are evaluated as the same color. This is because the cosine computation of the vector does not account for the length of a vector but only for its direction. An example for this would be an arbitrary color $c_1 = (r, g, b)$ and two colors $c_2 = (5, 10, 50)$ and $c_3 = 4 * c_2 = (10, 20, 100)$. Using the described property we know that $D_{\mathrm{C}}(c_1, c_2) = D_{\mathrm{C}}(c_1, c_3)$ thus, the segmentation between these pairs should be the same using D_{C}. We will investigate the two color pairs $P_3 = \{(20, 128, 90), c_2\}$ and $P_4 = \{(20, 128, 90), c_3\}$ using the three dissimilarity measures to see how they perform.
Furthermore, we will investigate how the measures fair on colors that some humans have trouble distinguishing. There are three main categories of color blindness red-green, blue-yellow and complete color blindness

[16]. As the names suggest, people with red-green (Deuteranomaly, Protanomaly, Protanopia, and Deuteranopia) and blue-yellow (Tritanomaly, Tritanopia) color blindness have a hard time or are unable to distinguish between the two colors. To test how the three dissimilarity measures perform with these colors we will test them on the color pairs $P_5 = \{(255, 0, 0), (0, 255, 0)\}$ and $P_6 = \{(0, 0, 255), (255, 255, 0)\}$. These represent red-green and blue-yellow, respectively.
This gives us the following color pairs to test with the synthetic images:

1. $P_1 = \{(200, 55, 0), (0, 55, 200)\}$
2. $P_2 = \{(120, 50, 50), (20, 255, 145)\}$
3. $P_3 = \{(20, 128, 90), (5, 10, 50)\}$
4. $P_4 = \{(20, 128, 90), (20, 40, 200)\}$
5. $P_5 = \{(255, 0, 0), (0, 255, 0)\}$
6. $P_6 = \{(0, 0, 255), (255, 255, 0)\}$

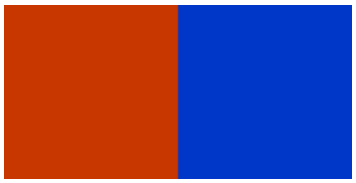

(a) Colors of pair 1.

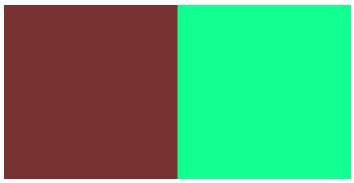

(b) Colors of pair 2.

(c) Colors of pair 3.

(d) Colors of pair 4.

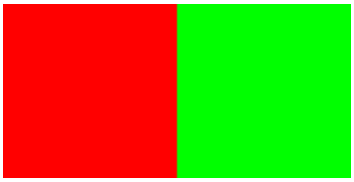

(e) Colors of pair 5.

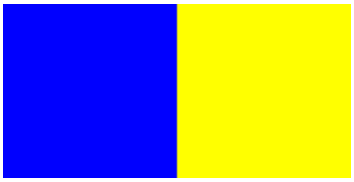

(f) Colors of pair 6.

Figure 7: Visualization of the 6 chosen color pairs.

4.1.2 Resulting Synthetic Images

To test the algorithm on the described color pairs, we have created a selection of images in which it is easy to see the correct separation. The images represent splits along the $\theta = \{0, \frac{\pi}{4}, \frac{\pi}{2}, \frac{3\pi}{4}\}$ directions. For each direction, we created two images, one with a transition region of thickness two along the segmentation line, and one without the transition region. The images using color pair P_1 can be seen in Figure 8. All other images can be found in section 7.

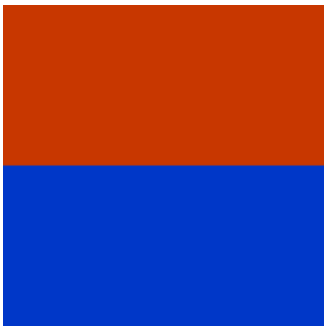

(a) Horizontal split ($\theta = 0$) without transition region.

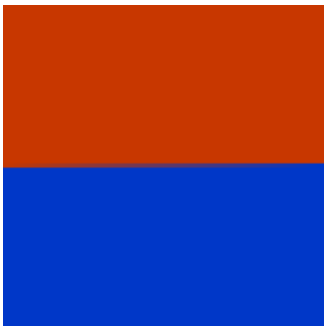

(b) Horizontal split ($\theta = 0$) with transition region.

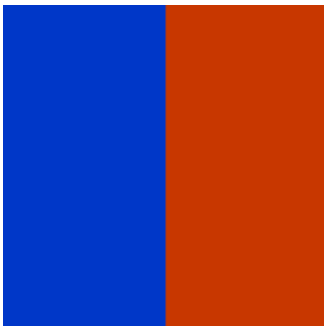

(c) Vertical split ($\theta = \frac{\pi}{2}$) without transition region.

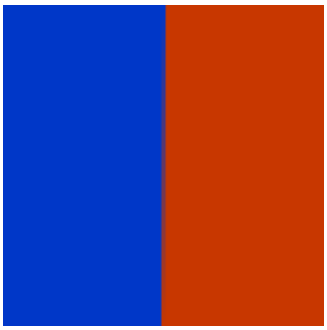

(d) Vertical split ($\theta = \frac{\pi}{2}$) with transition region.

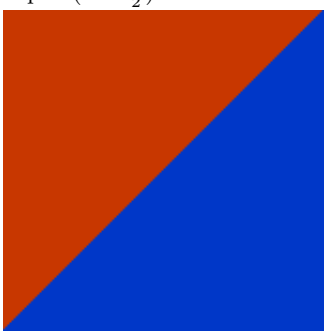

(e) Diagonal split from bottom left to top right ($\theta = \frac{\pi}{4}$) without transition region.

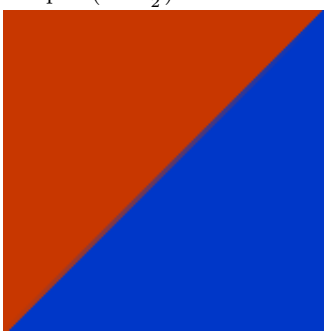

(f) Diagonal split from bottom left to top right ($\theta = \frac{\pi}{4}$) with transition region.

(g) Diagonal split from top left to bottom right ($\theta = \frac{3\pi}{4}$) without transition region.

(h) Diagonal split from top left to bottom ($\theta = \frac{3\pi}{4}$) right with transition region.

Figure 8: Synthetic images created for color pair P_1.

4.2 Real Satellite Data

To test the dissimilarity measures on real data, we used four images of the Zernike campus of the University of Groningen. These images show different campus regions (Figure 9). We can see that the images contain buildings, fields, trees, and roads. Hence, the data contains some high-detail structures and larger, more homogeneous, low-detail structures.
We will use ground truth images to see how well the dissimilarity measures perform on this data. These images were created by hand and show the different regions in the data in different colors. There are three different levels of detail in which these ground truth images have been created, all of which can be seen in Figure 10, Figure 11, Figure 12 and Figure 13. Depending on the level of detail, we can see that regions are either connected more broadly or separated at a lower level. We will compare the segmentation images produced using the different dissimilarity measures using subjective judgment, meaning we will compare them by eye. While this is not the most empiric method of determining the performance of the dissimilarity measures, it will give a useful insight into the performance trends of the measures. Implementing an objective, numerical measure that compares the segmentation images with the ground truth is beyond the scope of this research.

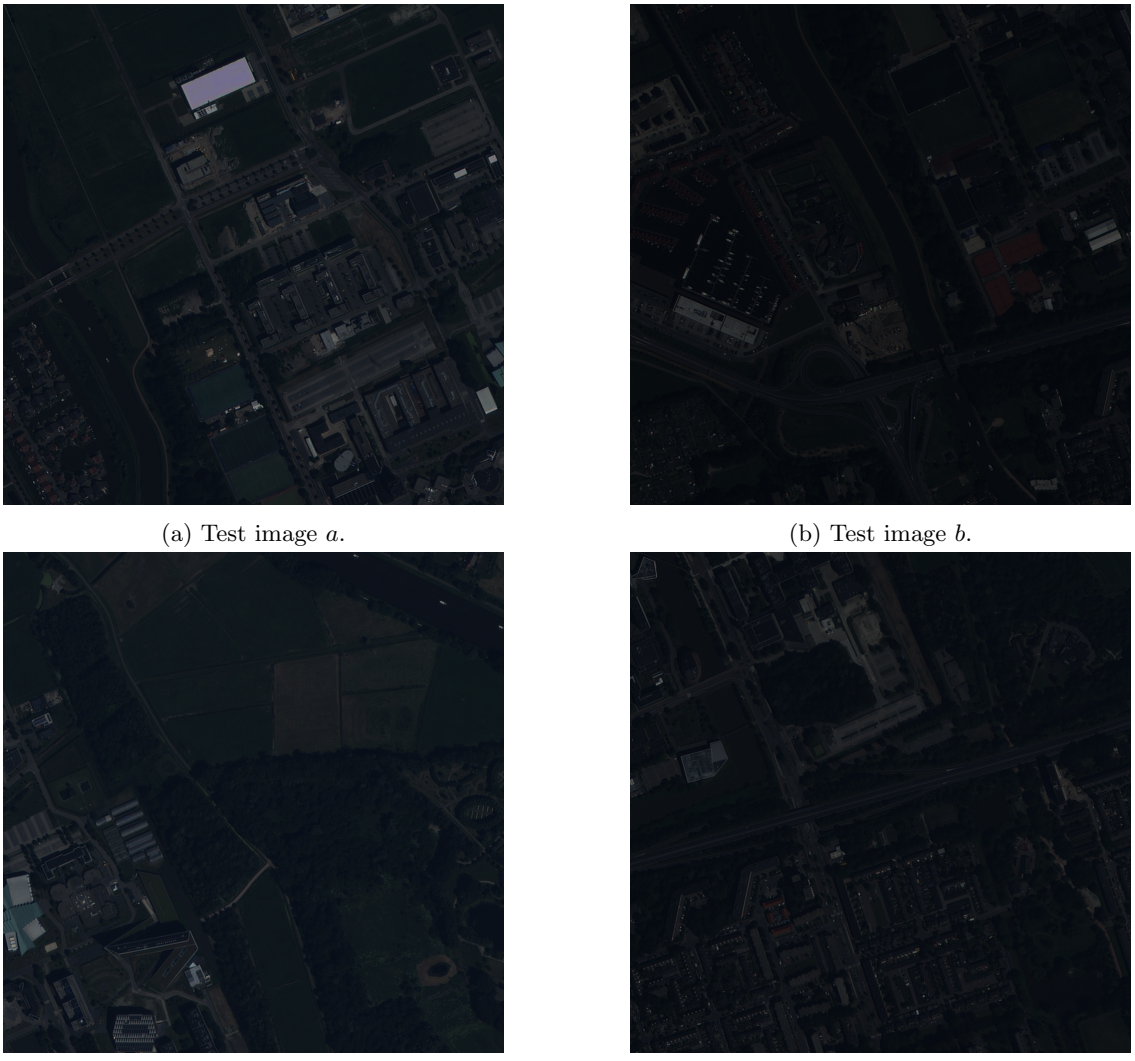

(a) Test image a.

(b) Test image b.

(c) Test image c.

(d) Test image d.

Figure 9: Satellite images of the Zernike campus used for testing the dissimilarity measures.

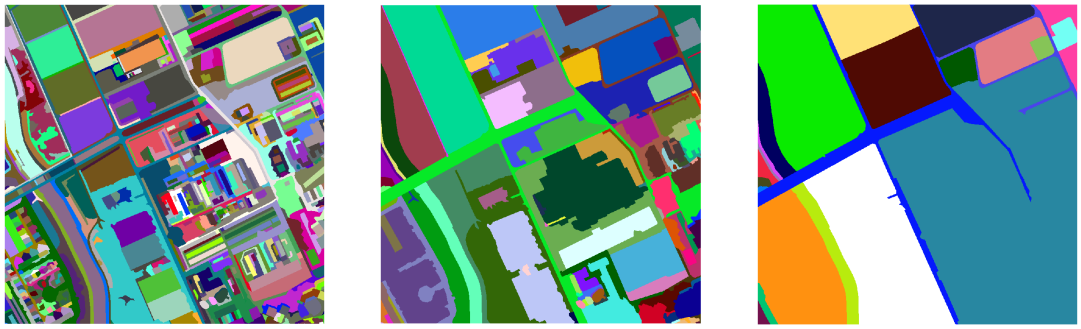

(a) High-level detail image. (b) Medium-level detail image. (c) Low-level detail image.

Figure 10: Ground truth images for test image *a*.

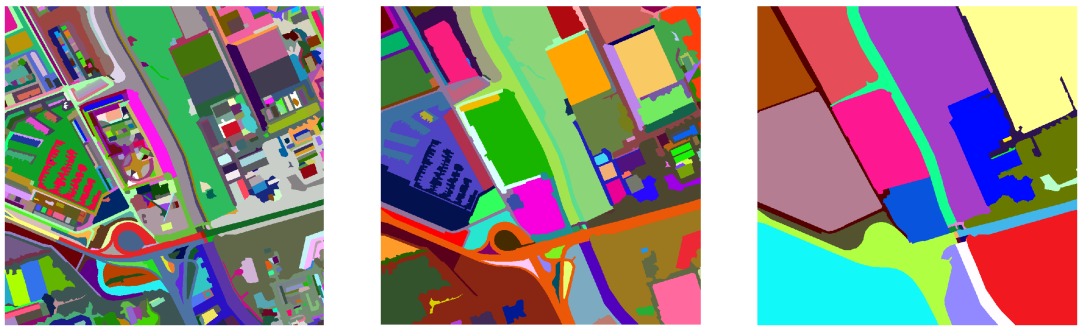

(a) High-level detail image. (b) Medium-level detail image. (c) Low-level detail image.

Figure 11: Ground truth images for test image *b*.

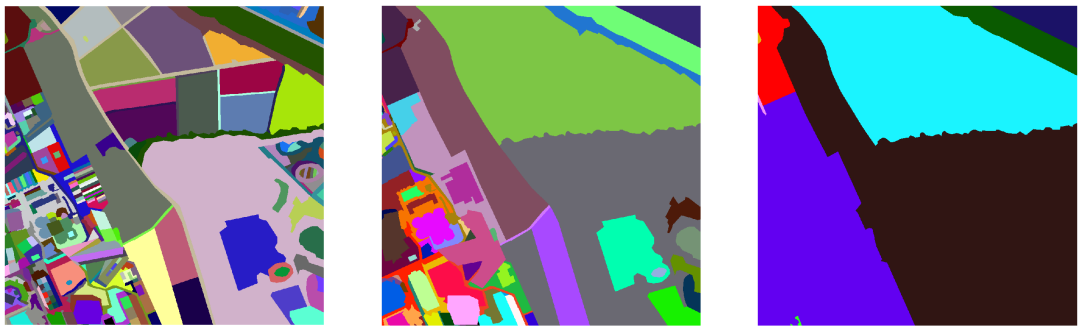

(a) High-level detail image. (b) Medium-level detail image. (c) Low-level detail image.

Figure 12: Ground truth images for test image *c*.

(a) High-level detail image. (b) Medium-level detail image. (c) Low-level detail image.

Figure 13: Ground truth images for test image d.

5 Results

In this section, we will present the segmentation of the three dissimilarity measures at a selection of alpha levels. First, we will show the results of the synthetic images. Second, we will show the results on the campus satellite data.

5.1 Synthetic Test Data

Before showing the algorithm's results on the synthetic data, we will list the distances between the used color pairs. We can see the raw dissimilarity scores in Table 1. Table 2 shows the dissimilarity scores mapped onto the range $[0, 10000]$ as defined in section 3.

Pair	D_{M}	D_{E}	D_{C}
P_1	400	282.84	0.9297
P_2	400	247.08	0.4530
P_3	173	125.50	0.2725
P_4	198	140.87	0.2725
P_5	510	360.62	1
P_6	765	441.67	1

Table 1: Non-normalized dissimilarity scores for the different color pairs.

Pair	D_{M}	D_{E}	D_{C}
P_1	5229	6403	9297
P_2	5229	5594	4530
P_3	2261	2841	2725
P_4	2588	3189	2725
P_5	6667	8165	10000
P_6	10000	10000	10000

Table 2: Normalized dissimilarity scores for the different color pairs.

5.1.1 Manhattan Distance

Based on the distances we have computed for the synthetic images, we expect the most accurate separation for color pair P_6. Color pairs P_3 and P_4 should have the least accurate segmentation and P_1, P_2 and P_5 should lie in between. As we can easily tell when the image is not segmented correctly anymore, we will

present the highest alpha value we can provide so that the images are still correctly separated. The results for each color pair can be seen in Table 3. The resulting segmentation images can be found in section 7.

Angle of Split	Transition Region	No Transition Region
$\theta = 0$	2627	5228
$\theta = \frac{\pi}{2}$	2627	5228
$\theta = \frac{\pi}{4}$	104	5228
$\theta = \frac{3\pi}{4}$	104	5228

(a) Maximum α value with successful separation for color pair P_1.

Angle of Split	Transition Region	No Transition Region
$\theta = 0$	2627	5228
$\theta = \frac{\pi}{2}$	2627	5228
$\theta = \frac{\pi}{4}$	104	5228
$\theta = \frac{3\pi}{4}$	104	5228

(b) Maximum α value with successful separation for color pair P_2.

Angle of Split	Transition Region	No Transition Region
$\theta = 0$	1137	2261
$\theta = \frac{\pi}{2}$	1137	2261
$\theta = \frac{\pi}{4}$	78	2261
$\theta = \frac{3\pi}{4}$	78	2261

(c) Maximum α value with successful separation for color pair P_3.

Angle of Split	Transition Region	No Transition Region
$\theta = 0$	2627	2588
$\theta = \frac{\pi}{2}$	2627	2588
$\theta = \frac{\pi}{4}$	52	2588
$\theta = \frac{3\pi}{4}$	52	2588

(d) Maximum α value with successful separation for color pair P_4.

Angle of Split	Transition Region	No Transition Region
$\theta = 0$	3359	6666
$\theta = \frac{\pi}{2}$	3359	6666
$\theta = \frac{\pi}{4}$	104	6666
$\theta = \frac{3\pi}{4}$	104	6666

(e) Maximum α value with successful separation for color pair P_5.

Angle of Split	Transition Region	No Transition Region
$\theta = 0$	5032	10000
$\theta = \frac{\pi}{2}$	5032	10000
$\theta = \frac{\pi}{4}$	156	10000
$\theta = \frac{3\pi}{4}$	156	10000

(f) Maximum α value with successful separation for color pair P_6.

Table 3: Maximum α value with successful separation for each color pair using D_{M}.

As a general observation, we can see that when no transition region is present, then the angle of the split does not influence the maximum α value that can be used for successful separation; the maximum α value is

equal to the distance of the used colors. The segmented images for input images without transition regions look equal to the input images.

For input images with a transition region, we see that the separation works better along the angles $\theta = 0$ and $\theta = \frac{\pi}{2}$. The maximum α value for these splits is significantly higher than for the angles $\theta = \frac{\pi}{4}$ and $\theta = \frac{3\pi}{4}$. Furthermore, we can see that the values with transition region for the pair $\theta = 0$, $\theta = \frac{\pi}{2}$ and the pair $\theta = \frac{\pi}{4}$, $\theta = \frac{3\pi}{4}$ are equal. It is likely that this result stems from us using the 4-α-CN and not the 8-α-CN, as the separation works well along the two angles used in the 4-α-CN approach.

When looking at the vertical and horizontal splits, all pairs have been segmented by assigning half of the transition region to one color and the other half to the other. For the diagonal splits the pairs P_1, P_2, P_4, P_5, P_6 have a segmentation in line with the gradient of the transition region. The segmented images have almost the same transition region as the original. An example for P_1 can be seen in Figure 14. Interestingly, for P_3 the transition region has been split into five equally sized parts that gradually transition from one color to the next for diagonal splits (Figure 15a, Figure 15b). Furthermore, we can see that P_4 is the only color where a split with a transition region has a higher α value than the split without a transition region (for the non-diagonal splits). Additionally, the α value for segmentation is higher or equal when the distance between the colors is higher, except for the diagonal split with transition region, where P_3 has a higher value than P_4 even though $D_{\mathrm{M}}(P_3) < D_{\mathrm{M}}(P_4)$.

(a) Diagonal split ($\theta = \frac{\pi}{4}$) at $\alpha = 104$.

(b) Diagonal split ($\theta = \frac{3\pi}{4}$) at $\alpha = 104$.

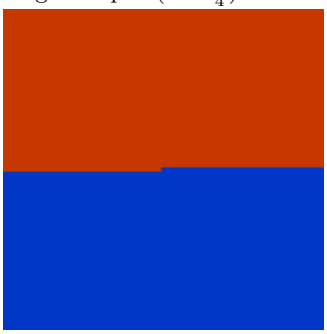

(c) Horizontal split ($\theta = 0$) at $\alpha = 2627$.

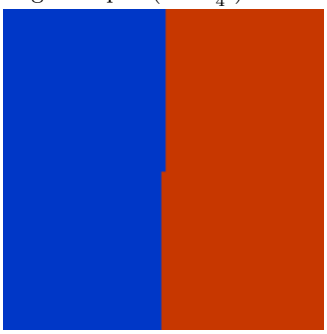

(d) Vertical split ($\theta = \frac{\pi}{2}$) at $\alpha = 2627$.

Figure 14: Resulting segmentation images for P_1 at maximal α value with transition regions using D_{M}.

(a) Diagonal split ($\theta = \frac{\pi}{4}$) at $\alpha = 78$.

(b) Diagonal split ($\theta = \frac{3\pi}{4}$) at $\alpha = 78$.

(c) Horizontal split ($\theta = 0$) at $\alpha = 1137$.

(d) Vertical split ($\theta = \frac{\pi}{2}$) at $\alpha = 1137$.

Figure 15: Resulting segmentation images for P_3 at maximal α value with transition regions using D_{M}.

5.1.2 Euclidean Distance

For the Euclidean distance we have seen that the relative distance of the color pairs is the same as for the Manhattan distance (Table 2), with the exception that $D_{\mathrm{E}}(P_1) > D_{\mathrm{E}}(P_2)$ while $D_{\mathrm{M}}(P_1) = D_{\mathrm{M}}(P_2)$. Consequently, we expect a similar order of segmentation quality for this dissimilarity measure. The maximum α values are expected to be higher than for D_{M}, as the distance of the colors in each color pair is consistently higher for D_{E} than for D_{M}. Again we will present the maximum α value for which the images have been successfully separated. The results for each color pair can be seen in Table 4. The resulting segmentation images can be found in section 7.

Angle of Split	Transition Region	No Transition Region
$\theta = 0$	3217	6403
$\theta = \frac{\pi}{2}$	3217	6403
$\theta = \frac{\pi}{4}$	128	6403
$\theta = \frac{3\pi}{4}$	128	6403

(a) Maximum α value with successful separation for color pair P_1.

Angle of Split	Transition Region	No Transition Region
$\theta = 0$	2811	5594
$\theta = \frac{\pi}{2}$	2811	5594
$\theta = \frac{\pi}{4}$	110	5594
$\theta = \frac{3\pi}{4}$	110	5594

(b) Maximum α value with successful separation for color pair P_2.

Angle of Split	Transition Region	No Transition Region
$\theta = 0$	1422	2841
$\theta = \frac{\pi}{2}$	1422	2841
$\theta = \frac{\pi}{4}$	78	2841
$\theta = \frac{3\pi}{4}$	78	2841

(c) Maximum α value with successful separation for color pair P_3.

Angle of Split	Transition Region	No Transition Region
$\theta = 0$	1608	3189
$\theta = \frac{\pi}{2}$	1608	3189
$\theta = \frac{\pi}{4}$	64	3189
$\theta = \frac{3\pi}{4}$	64	3189

(d) Maximum α value with successful separation for color pair P_4.

Angle of Split	Transition Region	No Transition Region
$\theta = 0$	4114	8164
$\theta = \frac{\pi}{2}$	4114	8164
$\theta = \frac{\pi}{4}$	128	8164
$\theta = \frac{3\pi}{4}$	128	8164

(e) Maximum α value with successful separation for color pair P_5.

Angle of Split	Transition Region	No Transition Region
$\theta = 0$	5032	10000
$\theta = \frac{\pi}{2}$	5032	10000
$\theta = \frac{\pi}{4}$	156	10000
$\theta = \frac{3\pi}{4}$	156	10000

(f) Maximum α value with successful separation for color pair P_6.

Table 4: Maximum α value with successful separation for each color pair using D_{E}.

Similarly to D_{M}, we see that for images not containing a transition region, the maximum α value is equal to the distance between the colors in the color pair. This is consistent across the four tested angles. The segmentation images without transition regions are identical to the input images.

Regarding the images with a transition region, we can again see that the performance was significantly better for the vertical and horizontal split than the diagonal split. When compared to D_{M} the α value is

either higher or equal for D_{E}. The segmentation images for the input images with transitions regions are split equally as for D_{M}. The horizontal and vertical transition regions are assigned one color for one half and the other color for the other half. This is consistent across all color pairs. For the diagonal splits we can again observe the split similar to the input image transition region for the color pairs P_1, P_2, P_4, P_5, P_6, while color pair P_3 again shows the five discrete regions. This is again visualized for P_1 and P_3 in Figure 16 and Figure 17.

(a) Diagonal split ($\theta = \frac{\pi}{4}$) at $\alpha = 128$.

(b) Diagonal split ($\theta = \frac{3\pi}{4}$) at $\alpha = 128$.

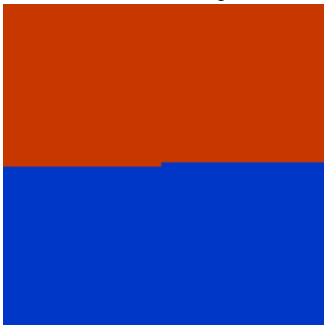

(c) Horizontal split ($\theta = 0$) at $\alpha = 3217$.

(d) Vertical split ($\theta = \frac{\pi}{2}$) at $\alpha = 3217$.

Figure 16: Resulting segmentation images for P_1 at maximal α value with transition regions using D_{E}.

(a) Diagonal split ($\theta = \frac{\pi}{4}$) at $\alpha = 78$.

(b) Diagonal split ($\theta = \frac{3\pi}{4}$) at $\alpha = 78$.

(c) Horizontal split ($\theta = 0$) at $\alpha = 1422$.

(d) Vertical split ($\theta = \frac{\pi}{2}$) at $\alpha = 1422$.

Figure 17: Resulting segmentation images for P_3 at maximal α value with transition regions using D_{E}.

5.1.3 Cosine Dissimilarity

For D_{C} we have seen a different relative distance of the different color pairs when compared to D_{M} and D_{E}. We expect the most accurate separation for P_5 and P_6, closely followed by P_1. P_3 and P_4 should have the least accurate separation and equal values because the color pairs have the same distance using D_{C}. D_{C} should perform better for P_2 then for P_3 and P_4 but worse than for the other three color pairs. As we can easily tell when the image is not segmented correctly anymore, we will present the highest alpha value we can provide so that the images are still correctly separated. The results for each color pair can be seen in Table 5. The resulting segmentation images can be found in section 7.

Angle of Split	Transition Region	No Transition Region
$\theta = 0$	2653	9296
$\theta = \frac{\pi}{2}$	2653	9296
$\theta = \frac{\pi}{4}$	3	9296
$\theta = \frac{3\pi}{4}$	3	9296

(a) Maximum α value with successful separation for color pair P_1.

Angle of Split	Transition Region	No Transition Region
$\theta = 0$	1167	4530
$\theta = \frac{\pi}{2}$	1167	4530
$\theta = \frac{\pi}{4}$	2	4530
$\theta = \frac{3\pi}{4}$	2	4530

(b) Maximum α value with successful separation for color pair P_2.

Angle of Split	Transition Region	No Transition Region
$\theta = 0$	682	2724
$\theta = \frac{\pi}{2}$	682	2724
$\theta = \frac{\pi}{4}$	3	2724
$\theta = \frac{3\pi}{4}$	3	2724

(c) Maximum α value with successful separation for color pair P_3.

Angle of Split	Transition Region	No Transition Region
$\theta = 0$	690	2724
$\theta = \frac{\pi}{2}$	690	2724
$\theta = \frac{\pi}{4}$	0	2724
$\theta = \frac{3\pi}{4}$	0	2724

(d) Maximum α value with successful separation for color pair P_4.

Angle of Split	Transition Region	No Transition Region
$\theta = 0$	2861	10000
$\theta = \frac{\pi}{2}$	2861	10000
$\theta = \frac{\pi}{4}$	2	10000
$\theta = \frac{3\pi}{4}$	2	10000

(e) Maximum α value with successful separation for color pair P_5.

Angle of Split	Transition Region	No Transition Region
$\theta = 0$	2861	10000
$\theta = \frac{\pi}{2}$	2861	10000
$\theta = \frac{\pi}{4}$	2	10000
$\theta = \frac{3\pi}{4}$	2	10000

(f) Maximum α value with successful separation for color pair P_6.

Table 5: Maximum α value with successful separation for each color pair using D_{C}.

Just like for the other two dissimilarity measures, we can see that for the images that do not have a transition region, the maximum α value corresponds to the distance value for the colors of the color pair. The segmentation images are again equal to the input images.

Surprisingly, this dissimilarity measure performed notably worse than the other two for the images with a diagonal split and a transition region. The maximum α value lies in the range $[0, 3]$ for all six color

pairs. Furthermore, the resulting segmentation images are different from the ones obtained using D_{M} and D_{E}. Instead of having a smooth transition between the colors, as for P_1, P_2, P_4, P_5 and P_6, and the 5 static transition regions, as for P_3, we obtained four different type of splits. For P_4, the image has the same transition region as the original image; this is expected, as the maximum α is zero, meaning that the image has no segmentation. For P_3, the transition region was separated into two solid strips of the two colors of the color pair, but the distribution of the colors is unequal. For both P_1 and P_5, the transition region was split into three equally sized parts. Two of them are the colors of the pair, while the middle section is the same as the original transition region at that point. For P_2 and P_5, the transition region was split into two sections. One of them has one of the colors of the pair, while the other is the same as the original transition region. The diagonal segmentation images for $\theta = \frac{\pi}{4}$ can be seen in Figure 18. The horizontal split images with a transition region have lower α values than the other two dissimilarity measures. The α values are in the order predicted for this dissimilarity measure, only that P_4 has a slightly higher value than P_3. The resulting images for $\theta = 0$ can be found in Figure 19, where we can see that the transition region was split into two sections, having either of the colors of the pair. These sections are only equally sized for P_1 and P_5. The separation is the same for $\theta = \frac{\pi}{2}$ only rotated.

(a) Diagonal split ($\theta = \frac{\pi}{4}$) at $\alpha = 3$ and P_1.

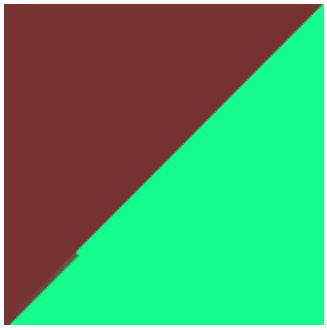

(b) Diagonal split ($\theta = \frac{\pi}{4}$) at $\alpha = 2$ and P_2.

(c) Diagonal split ($\theta = \frac{\pi}{4}$) at $\alpha = 3$ and P_3.

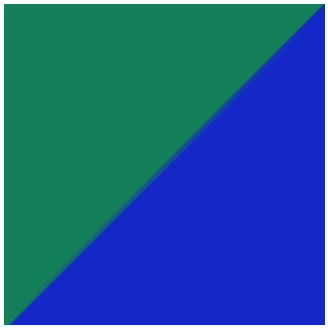

(d) Diagonal split ($\theta = \frac{\pi}{4}$) at $\alpha = 0$ and P_4.

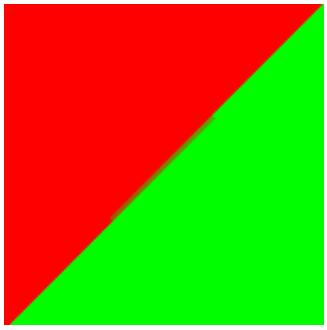

(e) Diagonal split ($\theta = \frac{\pi}{4}$) at $\alpha = 2$ and P_5.

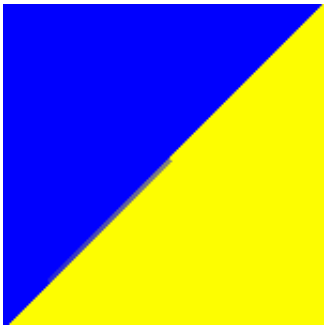

(f) Diagonal split ($\theta = \frac{\pi}{4}$) at $\alpha = 2$ and P_6.

Figure 18: Segmentation for the six color pairs at $\theta = \frac{\pi}{4}$ for different α values.

(a) Horizontal split ($\theta = 0$) at $\alpha =$ 2653 and P_1.

(b) Horizontal split ($\theta = 0$) at $\alpha =$ 1167 and P_1.

(c) Horizontal split ($\theta = 0$) at $\alpha =$ 682 and P_1.

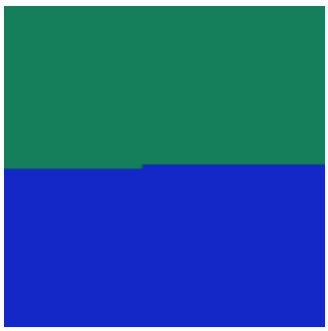

(d) Horizontal split ($\theta = 0$) at $\alpha =$ 690 and P_4.

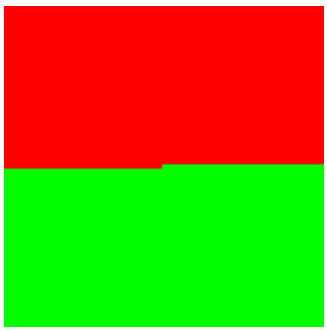

(e) Horizontal split ($\theta = 0$) at $\alpha =$ 2874 and P_5.

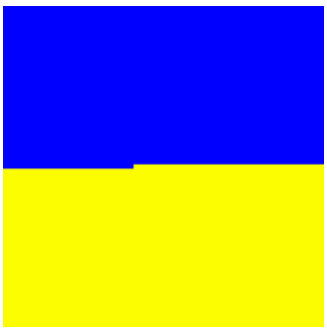

(f) Horizontal split ($\theta = 0$) at $\alpha =$ 2861 and P_6.

Figure 19: Segmentation for the six color pairs at $\theta = 0$ for different α values.

5.2 Satellite Data

We have seen that the diagonal splits with a transition region had the least accurate segmentation for all six color pairs we chose in the preliminary analysis. However, we expect these results to be the best predictors for appropriate α values in the satellite data, as it is likely that the real-life test data contains transition regions and that the separation of two colors will not lie along the x-axis or y-axis. The average α value for the synthetic images with a diagonal transition region are $\alpha = 100$ for D_{M}, $\alpha = 111$ for D_{E} and $\alpha = 2$ for D_{C}. We expect the appropriate α values of the three dissimilarity measures to lie around these averages.
The segmentation images presented in this section result from assigning a random color to every flat region identified by the α-tree algorithm. Furthermore, all flat regions containing less than ten pixels have been colored black, so they can easily be identified. We will mostly ignore these small regions and focus on the more significant flat regions identified by the algorithm.

5.2.1 General Trends

There are a few observations that are consistent across all four example pictures. Firstly, for all dissimilarity measures, we can see that setting the α value too low or too high results in segmentation images with either too many small flat regions or one large region. Either of these outcomes is not wanted. If the α value is too low, as seen in Figure 20, we observe that most of the image is black as most flat regions contain less than ten pixels. If the α value is too high, as seen in Figure 21, we observe that most of the image is one color. Having one large flat region like this removes most information about the structures we want to extract from the image. Therefore, we had to find an appropriate α value for each dissimilarity measure. It became apparent that D_{C} needed a significantly lower α value for achieving similar segmentation images as D_{E} and D_{M}, as predicted by the preliminary analysis.
Furthermore, the segmentation images using D_{C} were more sensitive to changes in α. Meanwhile, using D_{M} multiple α levels resulted in the same segmentation images. We compared the results to all ground truth images available and tried to find similarities between the ground truth images and the segmentation images.

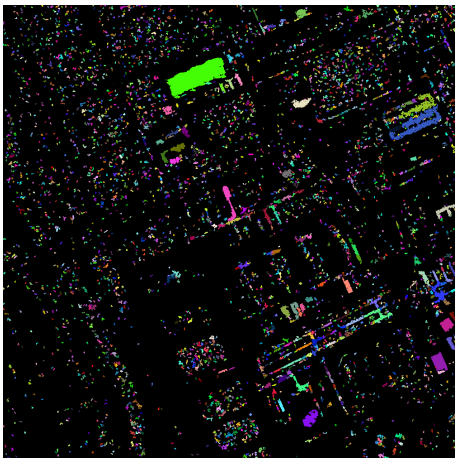

(a) Segmentation image using D_{C} at $\alpha = 1$.

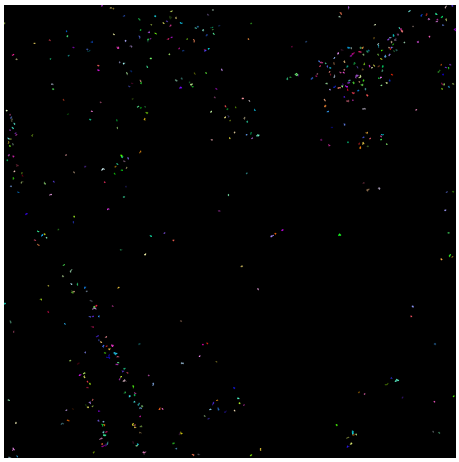

(b) Segmentation image using D_{E} at $\alpha = 20$.

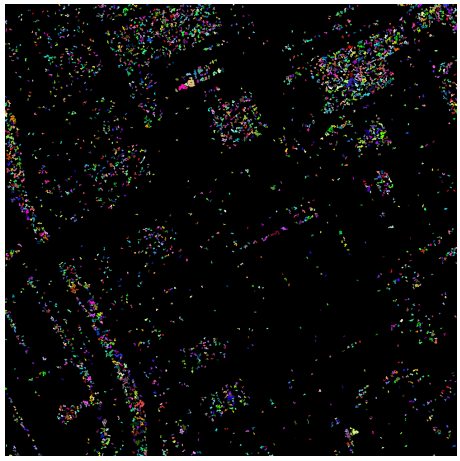

(c) Segmentation image using D_{M} at $\alpha = 20$.

Figure 20: Segmentation images using an α value that is too low on test image a.

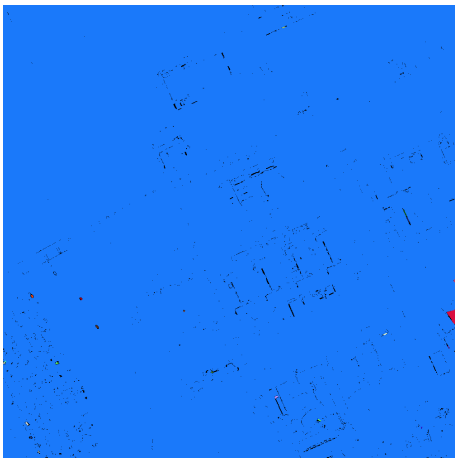

(a) Segmentation image using D_{C} at $\alpha = 100$.

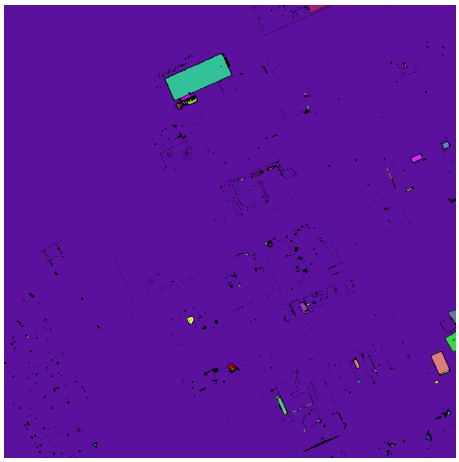

(b) Segmentation image using D_{E} at $\alpha = 600$.

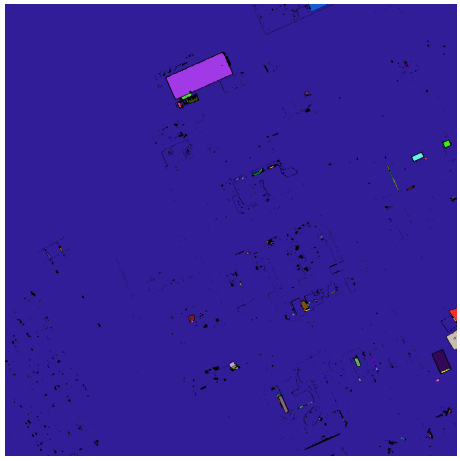

(c) Segmentation image using D_{E} at $\alpha = 600$.

Figure 21: Segmentation images using an α value that is too high on test image a.

5.2.2 Test Image a

For this test image the best segmentation was achieved at $\alpha = 5$ for D_{C}, $\alpha = 105$ for D_{E}, and $\alpha = 80$ for D_{M}. The resulting segmentation images and the ground truth images can be seen in Figure 22.
Regarding the results of D_{C} (Figure 22a), we see that a large section of the right side of the image has been combined into one flat region (muted purple), which does not correspond to any region in any of the ground truth images. At the top left of the image, we can see that four fields have been separated into different flat regions corresponding to section 1 in the high-detail ground truth image. At the bottom left of the image, we can see a green region corresponding to section 4 in the high-detail ground truth image. Additionally, we can see that three of the four sports fields have been separated, like in section 5 in the high-detail ground truth image. Lastly, we can see that the two buildings in sections 2 and 3 of the high-detail ground truth image have been segmented correctly as well.
When observing the results of D_{E} (Figure 22c), we see that the four fields at the top left of the image have been connected to one flat region, as can be seen in section 1 of the medium-detail ground truth image. However, section 2 of the medium-detail ground truth image was added to the region while being separate in all ground truth images. In the left half of the image, we can see three larger regions. The pink region at the top left corresponds reasonably well to section 3 of the medium-detail ground truth image. At the bottom left of the image, we can see a separation similar to sections 1 and 2 in the low-detail ground truth image. Sections 2 and 3 of the high-detail ground truth image have been segmented correctly. The rest of the image roughly matches section 6 of the high-detail ground truth image.

The results of D_{M} (Figure 22e) are very similar to the ones of D_{E}. However, section 2 of the medium-detail ground truth image has been correctly separated from section 1 of the medium-detail ground truth image. Additionally, the region that corresponds to section 2 of the low-detail ground truth image for D_{E} is more like section 4 of the medium-detail ground truth image for D_{M}. The rest of the image has roughly the same segmentation as D_{E}.

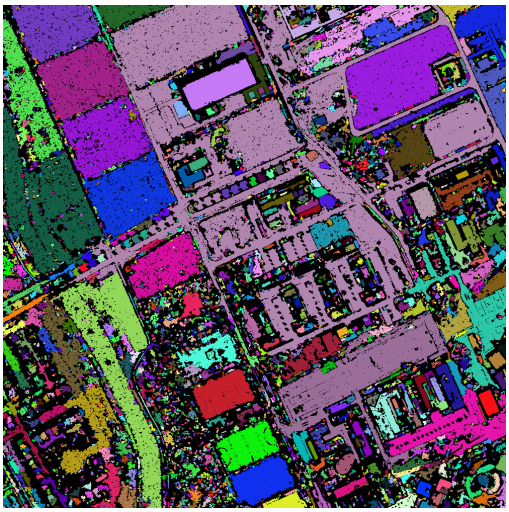

(a) Segmentation image using D_{C} at $\alpha = 5$.

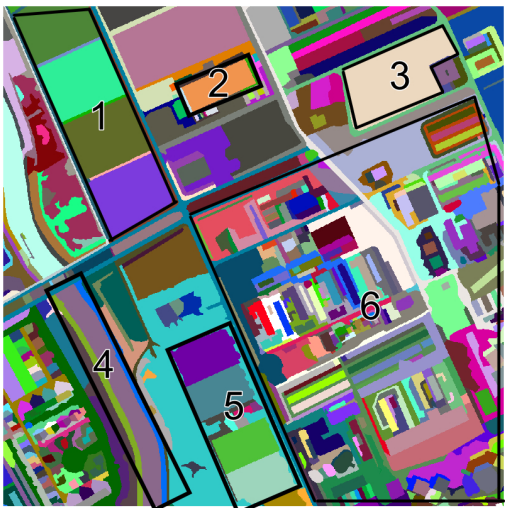

(b) Ground truth at high-detail level.

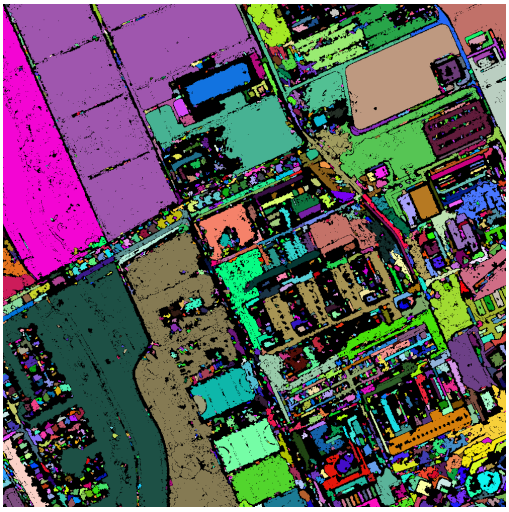

(c) Segmentation image using D_{E} at $\alpha = 105$.

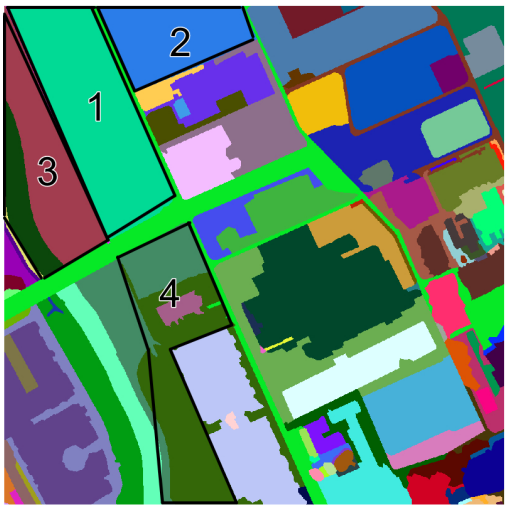

(d) Ground truth at medium-detail level.

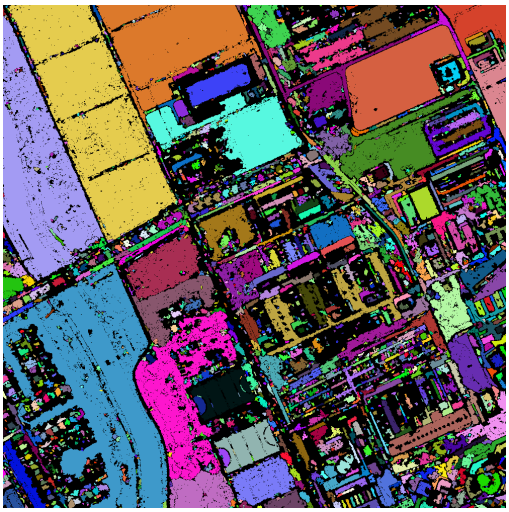

(e) Segmentation image using D_{M} at $\alpha = 80$.

(f) Ground truth at low-detail level.

Figure 22: Segmentation images using the three dissimilarity measures at different alpha levels and ground truth images for test image a.

5.2.3 Test Image *b*

For this test image the best segmentation was achieved at $\alpha = 12$ for D_{C}, $\alpha = 85$ for D_{E}, and $\alpha = 65$ for D_{M}. The resulting segmentation images and the ground truth images can be seen in Figure 23.
The results of D_{C} (Figure 23a) have only a few similarities to the ground truth images. We see a yellow section roughly corresponding to section 1 of the medium-detail ground truth image. Furthermore, one of the buildings in section 1 of the high-detail ground truth image has been identified. Lastly, a pink region corresponds to section 6 of the medium-detail ground truth image, but it is too large. Other than that, no regions correspond well to the sections in the ground truth images.
The segmentation image using D_{E} (Figure 23c) has more similarities to the ground truth images. We can see that the green part of section 2 of the high-detail ground truth image has been well segmented. Also, at the bottom left of the image, we can see a purple region corresponding to section 3 of the low-detail ground truth image. On the right side of the image, we see a light blue region that combines sections 1 and 2 of the low-detail ground truth image. Moreover, we can see two regions corresponding to section 5 and section 6 of the medium-detail ground truth image. Similarly to D_{C} we see a green region that combines section 1 and section 3 of the medium-detail ground truth image.
For D_{M} (Figure 23e) we can again see many similarities to D_{E} but with a bit more detail. We can see a region combining section 2 of the medium-detail ground truth image and section 2 of the low-detail ground truth image. Section 2 and section 3 of the high-detail ground truth image and section 5 of the medium-detail ground truth image have been clearly segmented. We again observe a region that combines section 1 and section 3 of the medium-detail ground truth image, but it is more similar to the ground truth than the region for D_{E} as we can also see section 5 of the high-detail ground truth image. At the bottom left, we can see two regions roughly corresponding to section 4 of the high-detail ground truth image and section 4 of the medium-detail ground truth image.

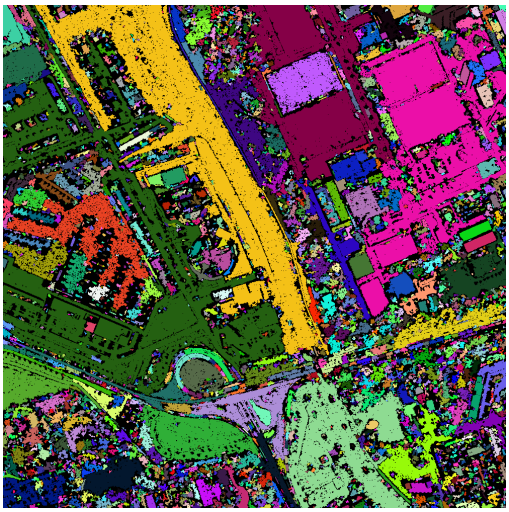

(a) Segmentation image using D_{C} at $\alpha = 12$.

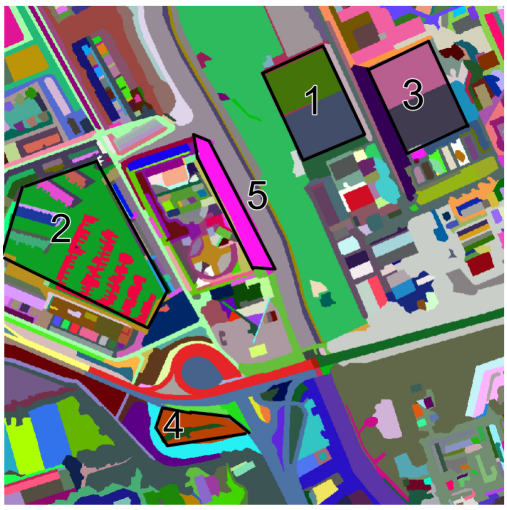

(b) Ground truth at high-detail level.

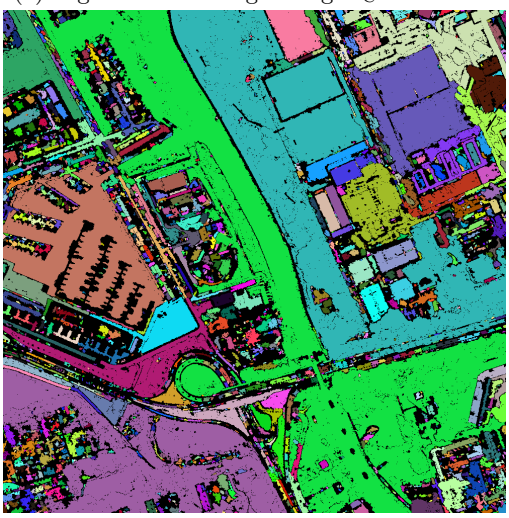

(c) Segmentation image using D_{E} at $\alpha = 85$.

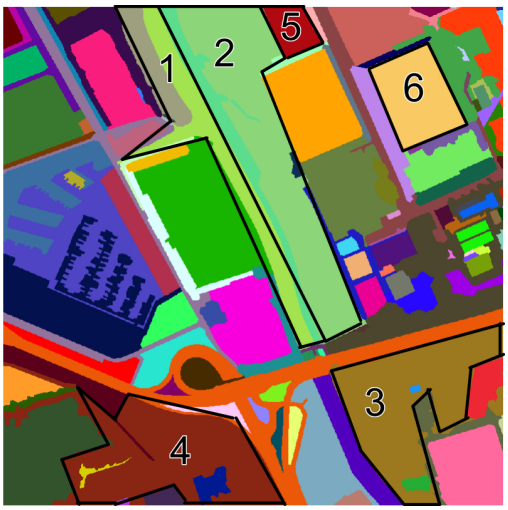

(d) Ground truth at medium-detail level.

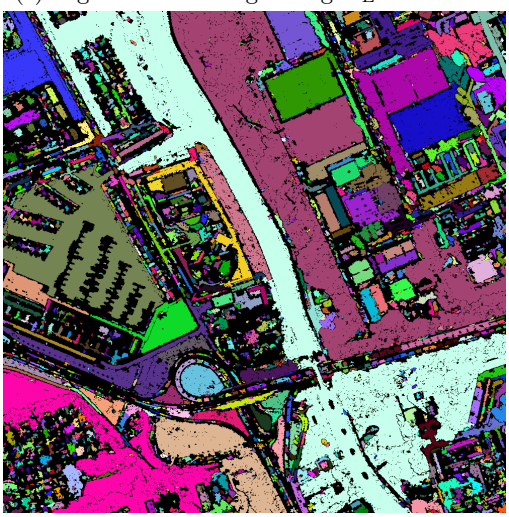

(e) Segmentation image using D_{M} at $\alpha = 65$.

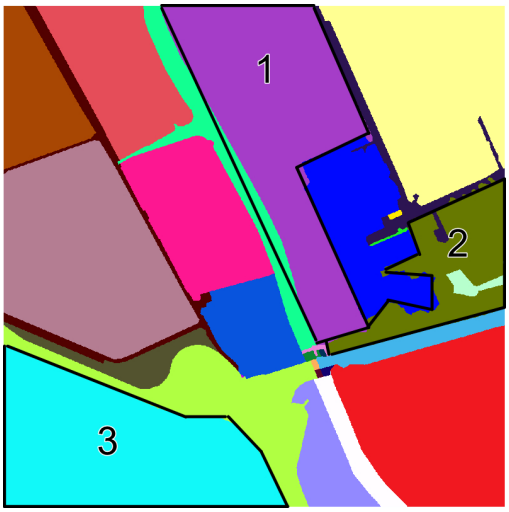

(f) Ground truth at low-detail level.

Figure 23: Segmentation images using the three dissimilarity measures at different alpha levels and ground truth images for test image *b*.

5.2.4 Test Image *c*

For this test image the best segmentation was achieved at $\alpha = 3$ for D_{C}, $\alpha = 75$ for D_{E}, and $\alpha = 65$ for D_{M}. The resulting segmentation images and the ground truth images can be seen in Figure 24.
In the results of D_{C} (Figure 24a) for this test image, we see that the fields from section 1 in the high-detail ground truth image have been relatively well segmented. Some are connected into one flat region, but they are mostly recognizable. Furthermore, we can see that section 3 and section 5 of the high-detail ground truth image have been well segmented. Additionally, many details of section 4 of the high-detail ground truth image have been preserved. The primarily black regions, which were forests in the original image, are not marked as one coherent region.
Regarding D_{E} (Figure 24c), we can again see fairly well-segmented regions for section 1 of the high-detail ground truth image. However, there are more merged fields, and some regions that should be connected are not. Section 5 of the high-detail ground truth image has again been segmented well. The detail in section 4 of the high-detail ground truth image can still be seen but is not as well reproduced. In contrast to D_{C} using this measure, we found a region fairly well encapsulating section 1 of the medium-detail ground truth image and a region corresponding to section 2 of the high-detail ground truth image. Nevertheless, the region that corresponded to section 3 of the high-detail ground truth image for D_{C} now has its regions merged and corresponds more to section 2 of the medium-detail ground truth image, and the region has a fairly large error on the right.
The results of D_{M} (Figure 24e) again show some segmentation of the fields of section 1 of the high-detail ground truth image. However, many disruptions in the fields can be seen as the least accurate segmentation of that section between the three measures. Section 2 and section 5 of the high-detail ground truth image have been clearly segmented from the rest of the image. As for D_{E}, section 2 of the medium-detail ground truth image has been segmented, but it does not contain the large error. The level of detail for section 4 of the high-detail ground truth image is roughly the same as for D_{E}.

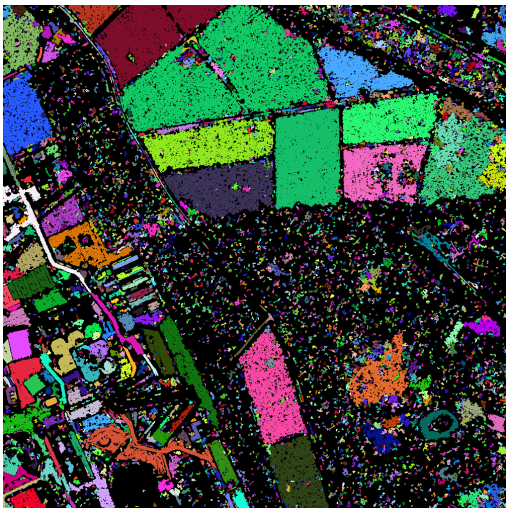

(a) Segmentation image using D_{C} at $\alpha = 3$.

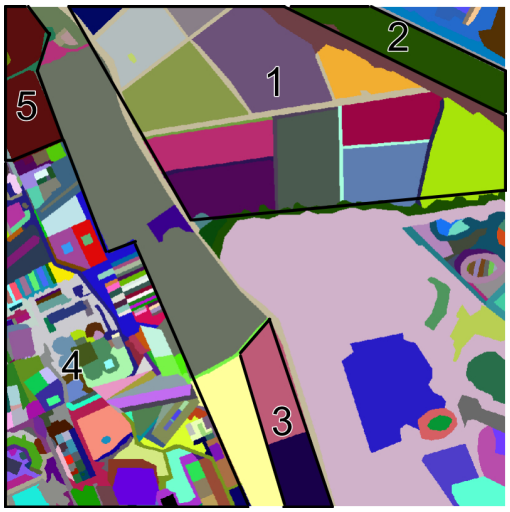

(b) Ground truth at high-detail level.

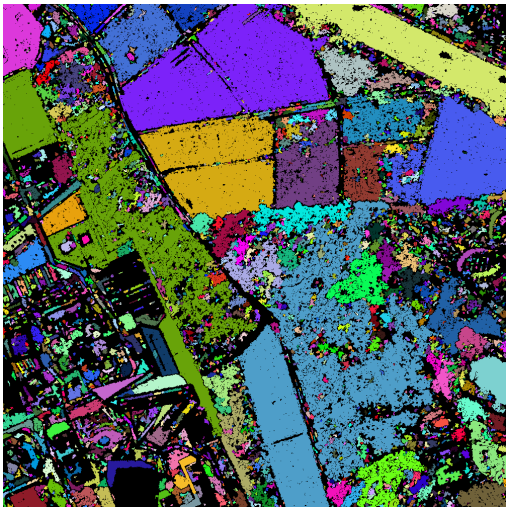

(c) Segmentation image using D_{E} at $\alpha = 75$.

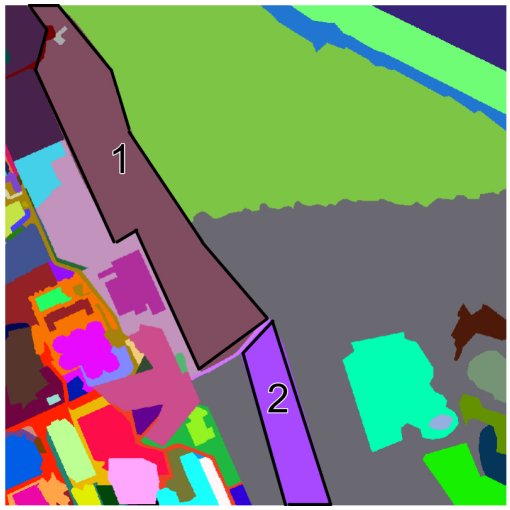

(d) Ground truth at medium-detail level.

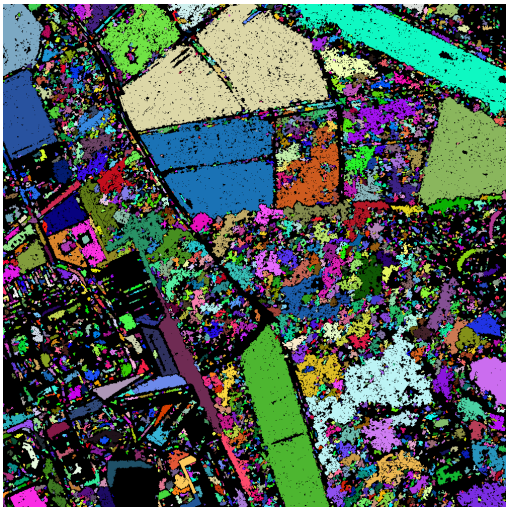

(e) Segmentation image using D_{M} at $\alpha = 65$.

(f) Ground truth at low-detail level.

Figure 24: Segmentation images using the three dissimilarity measures at different alpha levels and ground truth images for test image c.

5.2.5 Test Image *d*

For this test image the best segmentation was achieved at $\alpha = 11$ for D_{C}, $\alpha = 90$ for D_{E}, and $\alpha = 75$ for D_{M}. The resulting segmentation images and the ground truth images can be seen in Figure 25.
One prominent region we can see in yellow for the results of D_{C} (Figure 25a) combines sections 2, 3, and 4 of the low-detail ground truth image. We can also see that this measure segmented section 1 from the low-detail image while merging the larger and smaller part of that section into one region. In the bottom half of the image, we can see that there is one region in dark blue that corresponds to section 4 of the medium-detail ground truth image. Also, we see that section 3 of the medium-detail ground truth image has been split into two regions. Some of the detail in section 2 of the high-detail ground truth image has been preserved, but a few larger regions can be seen in the results but not in the ground truth image.
The segmentation using D_{E} (Figure 25c) found one region that accurately corresponds to section 2 of the low-detail ground truth image. Furthermore, we can see that sections 1 and 2 of the medium-detail ground truth image have been segmented well. Sections 3 and 4 have been combined into one larger region. We can also observe that most of the detail of sections 1 and 2 of the high-detail ground truth image has been preserved.
Once more we can see that the results of D_{E} and D_{M} (Figure 25e) are quite similar. The region that corresponds to section 2 of the low-detail ground truth image has been split into one larger and two smaller regions. Additionally, sections 3 and 4 are separately segmented using this dissimilarity measure. Finally, we see that sections 1 and 2 of the medium-detail ground truth image and sections 1 and 2 of the high-detail ground truth image have been well segmented.

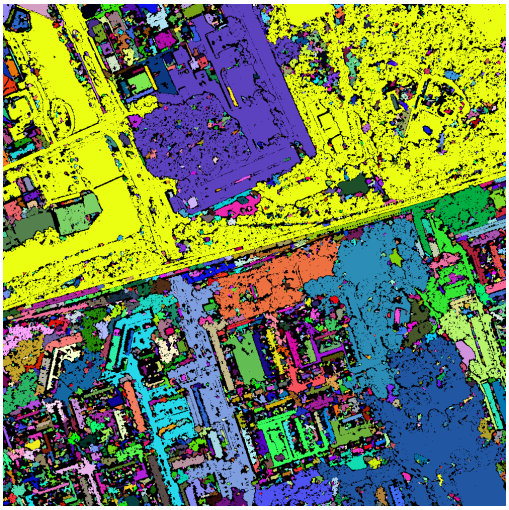

(a) Segmentation image using D_{C} at $\alpha = 11$.

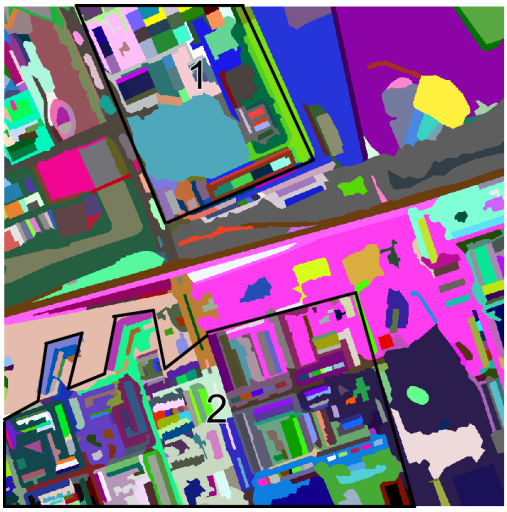

(b) Ground truth at high-detail level.

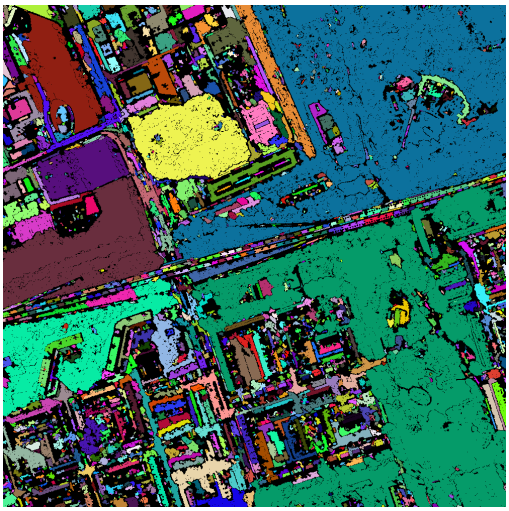

(c) Segmentation image using D_{E} at $\alpha = 90$.

(d) Ground truth at medium-detail level.

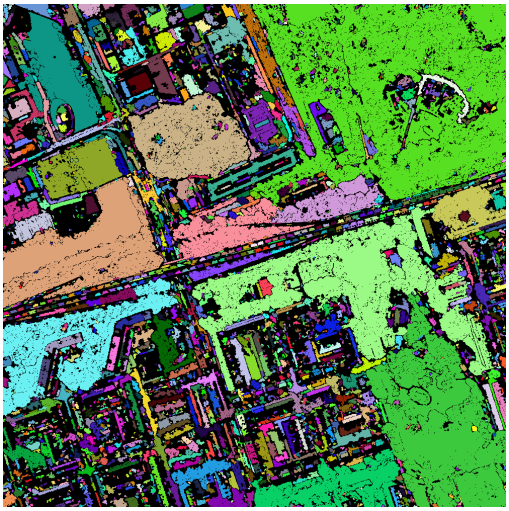

(e) Segmentation image using D_{M} at $\alpha = 75$.

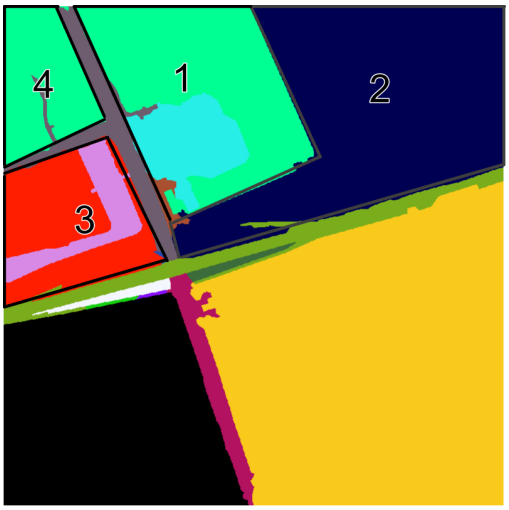

(f) Ground truth at low-detail level.

Figure 25: Segmentation images using the three dissimilarity measures at different alpha levels and ground truth images for test image d.

6 Discussion

The goal of this research is to establish appropriate α values for the three dissimilarity measures; the Manhattan distance D_{M}, the Euclidean distance D_{E} and the cosine distance D_{C} that can be used for image segmentation. Furthermore, it should be assessed how well the dissimilarity measures can detect relevant sections in the provided sample images. Evaluating the dissimilarity measures is beneficial to apply the α-tree algorithm to colored images, which can be used in agriculture, disaster management, and pollution detection.

For D_{M} we have found that the most appropriate images were created at an α level in the range of $[60, 80]$. This range is lower than the predicted value of 100 but reasonably close. The segmentation images were most similar to the medium detail ground truth images. In addition to identifying these medium-sized structures, the dissimilarity measure was able to segment buildings in a building complex, as in test images *a* and *d*. D_{M} did not seem appropriate to identify coarse regions, like in the low-detail ground truth images.

Regarding D_{E} an α level in the range of $[70, 110]$ produced appropriate segmentation images. This range corresponds well to the predicted value of 110. The segmentation images were most similar to the medium detail ground truth images. As for D_{M}, the segmentation images were most similar to the medium detail ground truth images while still able to segment detailed structures as buildings. However, the segmentation images using D_{E} had a little bit less detail and were more likely to connect neighboring sections into one, compared to D_{M}.

The dissimilarity measure D_{C} had a considerably lower appropriate α level range of $[3, 15]$. The predicted value of 2 is close to this range but lower. It also became apparent that a change in α value had a more considerable impact on the resulting segmentation image for D_{C} than this exact change would have for the other two dissimilarity measures. We expect the colors in the test images to be an explanation for this difference. The test images primarily show fields, buildings, roads, and trees. Hence, they contain many shades of green and gray. One property of D_{C} is that given two shades of the same color, such as $(1, 1, 1)$ and $(100, 100, 100)$, then these shades are evaluated as the same color using D_{C}. On the contrary, the other two dissimilarity measures would detect a difference between these colors. Therefore, given sample images with multiple shades of the same colors, a slight change in α would significantly increase the size of connected components in the segmentation images for D_{C}.

Generally, we observed that the appropriate α levels are low for all dissimilarity measures compared to the possible range of $[0, 10000]$. We could observe that the α values of the synthetic images with diagonal transition regions served well as a predictor of appropriate α values in the satellite data. The α values are possibly so low since we used the RGB color space. As described before, the test images contain many shades of green and gray. Using the three dissimilarity measures, different shades of the same color are relatively close in the RGB color space. Due to this proximity, the α levels needed to be relatively low to differentiate between similar colors correctly. An exciting venture for future research would be to represent the images in different color spaces and see how that influences the appropriate α value range.
Interestingly, none of the dissimilarity measures correctly identified the forest section in test image *c*. While the trees seem similar in color, their high variance in structure might have hindered the algorithm from correctly identifying them as one region. Future research could focus on adding steps in the algorithm that connects structurally similar regions. This could be done by adjusting a pixel's neighborhood in the algorithm's comparison phase or applying a different or adjusted dissimilarity measure.
Furthermore, future research should employ objective, numerical measures to assess the similarity between the segmentation created by the algorithm and the ground truth images. A numerical value would allow us to compare the performance of different dissimilarity measures. Two measures that could be used for this task are precision and recall of overlapping regions between the ground truth images and the created segmentation images.

References

[1] S. Andrilli and D. Hecker. Chapter 1 - vectors and matrices. In S. Andrilli and D. Hecker, editors, *Elementary Linear Algebra (Fourth Edition)*, pages 1–77. Academic Press, Boston, fourth edition edition, 2010.

[2] S.-H. Cha, S. Yoon, and C. C. Tappert. Enhancing binary feature vector similarity measures. Technical report, Pace university, 2005.

[3] R. Gerhards and H. Oebel. Practical experiences with a system for site-specific weed control in arable crops using real-time image analysis and gps-controlled patch spraying. *Weed research*, 46(3):185–193, 2006.

[4] R. M. Haralick and L. G. Shapiro. Image segmentation techniques. *Computer Vision, Graphics, and Image Processing*, 29(1):100–132, 1985.

[5] G. H. Joblove and D. Greenberg. Color spaces for computer graphics. In *Proceedings of the 5th annual conference on Computer graphics and interactive techniques*, pages 20–25, 1978.

[6] S. Kshirsagar, S. Ghodke, and R. Shriram. Ocean pollution detection using image processing. In *2021 International Conference on Emerging Smart Computing and Informatics (ESCI)*, pages 408–412. IEEE, 2021.

[7] G. K. Ouzounis and P. Soille. *The Alpha-Tree algorithm*. Publications Office of the European Union, Dec. 2012.

[8] A. Procházka, M. Kolinova, J. Fiala, P. Hampl, and K. Hlavaty. Satellite image processing and air pollution detection. In *2000 IEEE International Conference on Acoustics, Speech, and Signal Processing. Proceedings (Cat. No. 00CH37100)*, volume 4, pages 2282–2285. IEEE, 2000.

[9] F. Rahutomo, T. Kitasuka, and M. Aritsugi. Semantic cosine similarity. In *The 7th International Student Conference on Advanced Science and Technology ICAST*, volume 4, page 1, 2012.

[10] G. Salton and C. Buckley. Term-weighting approaches in automatic text retrieval. *Information processing & management*, 24(5):513–523, 1988.

[11] J. Silva, N. Varela, and O. B. P. Lezama. Multispectral image analysis for the detection of diseases in coffee production. In *International Symposium on Distributed Computing and Artificial Intelligence*, pages 198–205. Springer, 2020.

[12] P. Soille. Constrained connectivity for hierarchical image partitioning and simplification. *IEEE transactions on pattern analysis and machine intelligence*, 30(7):1132–1145, 2008.

[13] P. Soille. Preventing chaining through transitions while favouring it within homogeneous regions. In *International Symposium on Mathematical Morphology and Its Applications to Signal and Image Processing*, pages 96–107. Springer, 2011.

[14] P. Soille and J. Grazzini. Constrained connectivity and transition regions. In *International Symposium on Mathematical Morphology and Its Applications to Signal and Image Processing*, pages 59–69. Springer, 2009.

[15] S. Voigt, T. Kemper, T. Riedlinger, R. Kiefl, K. Scholte, and H. Mehl. Satellite image analysis for disaster and crisis-management support. *IEEE transactions on geoscience and remote sensing*, 45(6):1520–1528, 2007.

[16] G. Wald and P. K. Brown. Human color vision and color blindness. In *Cold Spring Harbor symposia on quantitative biology*, volume 30, pages 345–361. Cold Spring Harbor Laboratory Press, 1965.

[17] X. Zhang and M. Wilkinson. Preventing chaining in alpha-trees using gabor filters. In B. Burgeth, A. Kleefeld, B. Naegel, N. Passat, and B. Perret, editors, *Mathematical Morphology and Its Applications to Signal and Image Processing*, Lecture Notes in Computer Science, pages 268–280. Springer, jul 2019. International Symposium on Mathematical Morphology, ISMM ; Conference date: 08-07-2019 Through 10-07-2019.

7 Appendix

7.1 Synthetic Test Images

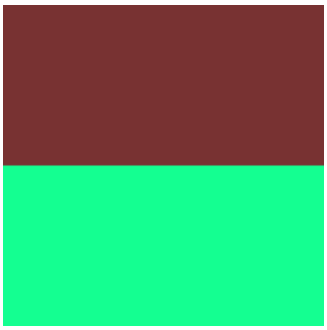

(a) Horizontal split ($\theta = 0$) without transition region.

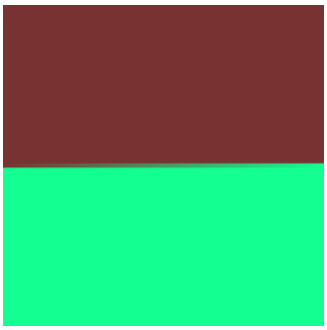

(b) Horizontal split ($\theta = 0$) with transition region.

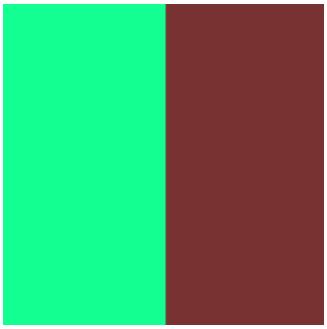

(c) Vertical split ($\theta = \frac{\pi}{2}$) without transition region.

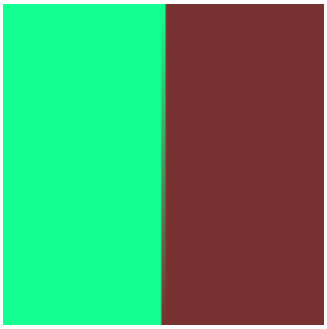

(d) Vertical split ($\theta = \frac{\pi}{2}$) with transition region.

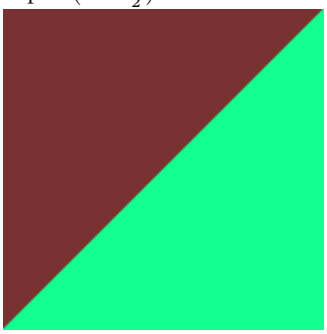

(e) Diagonal split from bottom left to top right ($\theta = \frac{\pi}{4}$) without transition region.

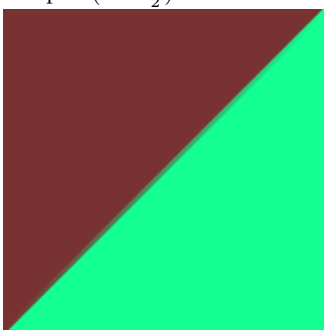

(f) Diagonal split from bottom left to top right ($\theta = \frac{\pi}{4}$) with transition region.

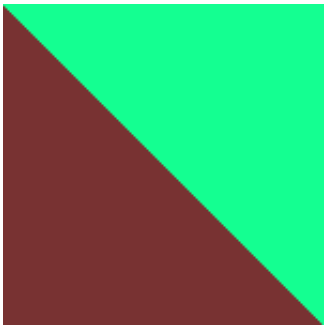

(g) Diagonal split from top left to bottom right ($\theta = \frac{3\pi}{4}$) without transition region.

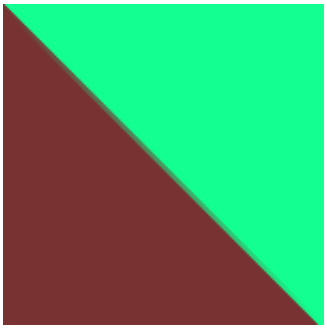

(h) Diagonal split from top left to bottom ($\theta = \frac{3\pi}{4}$) right with transition region.

Figure 26: Synthetic images created for color pair P_2.

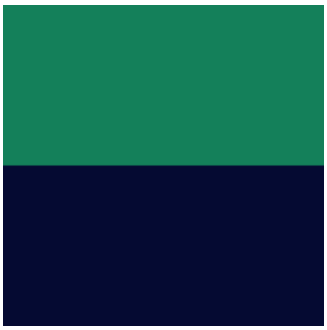

(a) Horizontal split ($\theta = 0$) without transition region.

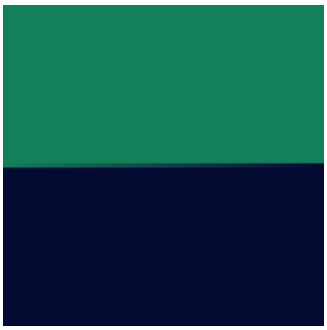

(b) Horizontal split ($\theta = 0$) with transition region.

(c) Vertical split ($\theta = \frac{\pi}{2}$) without transition region.

(d) Vertical split ($\theta = \frac{\pi}{2}$) with transition region.

(e) Diagonal split from bottom left to top right ($\theta = \frac{\pi}{4}$) without transition region.

(f) Diagonal split from bottom left to top right ($\theta = \frac{\pi}{4}$) with transition region.

(g) Diagonal split from top left to bottom right ($\theta = \frac{3\pi}{4}$) without transition region.

(h) Diagonal split from top left to bottom ($\theta = \frac{3\pi}{4}$) right with transition region.

Figure 27: Synthetic images created for color pair P_3.

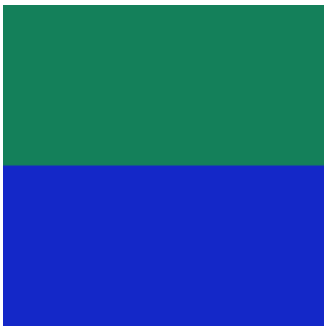

(a) Horizontal split ($\theta = 0$) without transition region.

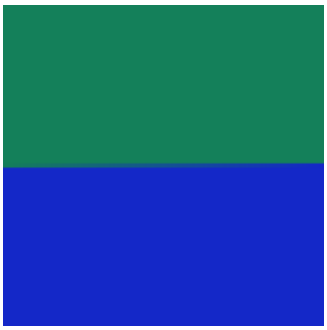

(b) Horizontal split ($\theta = 0$) with transition region.

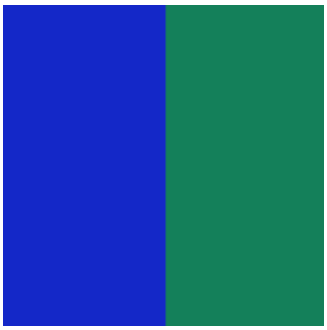

(c) Vertical split ($\theta = \frac{\pi}{2}$) without transition region.

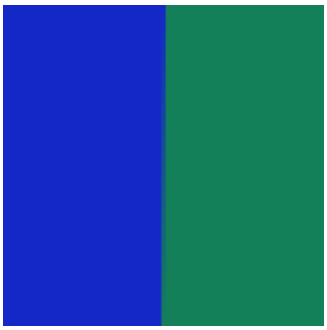

(d) Vertical split ($\theta = \frac{\pi}{2}$) with transition region.

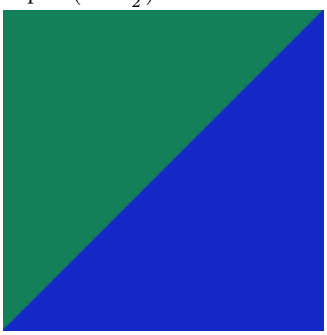

(e) Diagonal split from bottom left to top right ($\theta = \frac{\pi}{4}$) without transition region.

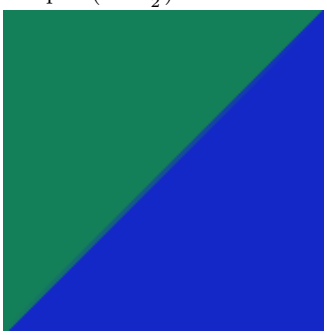

(f) Diagonal split from bottom left to top right ($\theta = \frac{\pi}{4}$) with transition region.

(g) Diagonal split from top left to bottom right ($\theta = \frac{3\pi}{4}$) without transition region.

(h) Diagonal split from top left to bottom ($\theta = \frac{3\pi}{4}$) right with transition region.

Figure 28: Synthetic images created for color pair P_4.

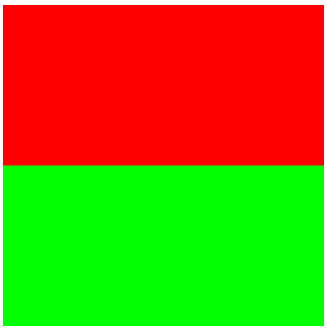

(a) Horizontal split ($\theta = 0$) without transition region.

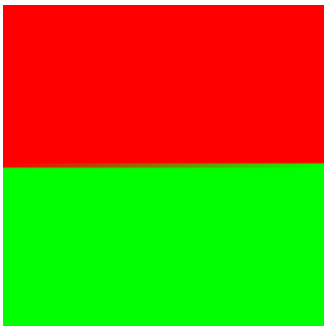

(b) Horizontal split ($\theta = 0$) with transition region.

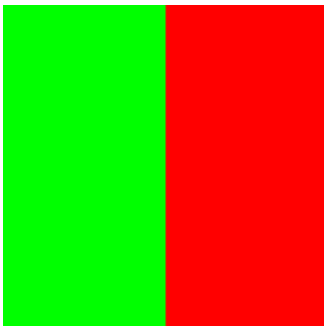

(c) Vertical split ($\theta = \frac{\pi}{2}$) without transition region.

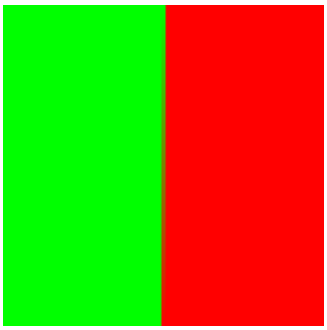

(d) Vertical split ($\theta = \frac{\pi}{2}$) with transition region.

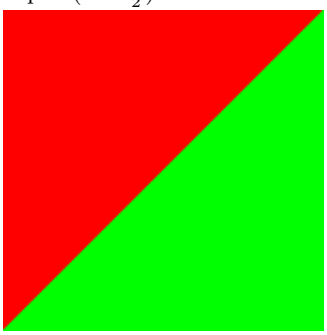

(e) Diagonal split from bottom left to top right ($\theta = \frac{\pi}{4}$) without transition region.

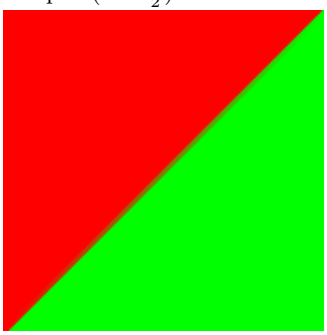

(f) Diagonal split from bottom left to top right ($\theta = \frac{\pi}{4}$) with transition region.

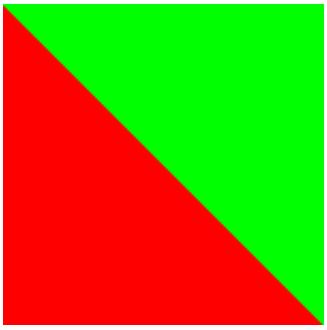

(g) Diagonal split from top left to bottom right ($\theta = \frac{3\pi}{4}$) without transition region.

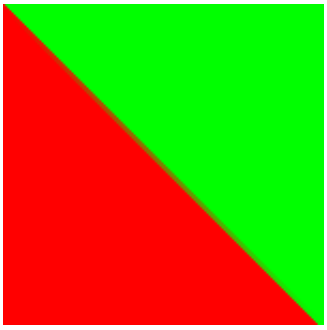

(h) Diagonal split from top left to bottom ($\theta = \frac{3\pi}{4}$) right with transition region.

Figure 29: Synthetic images created for color pair P_5.

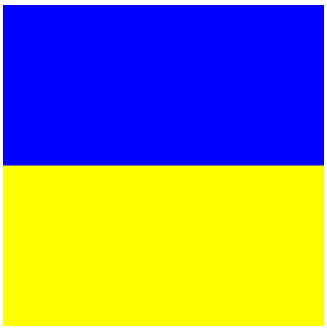

(a) Horizontal split ($\theta = 0$) without transition region.

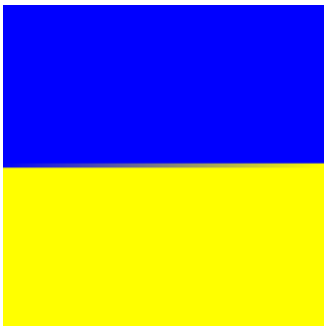

(b) Horizontal split ($\theta = 0$) with transition region.

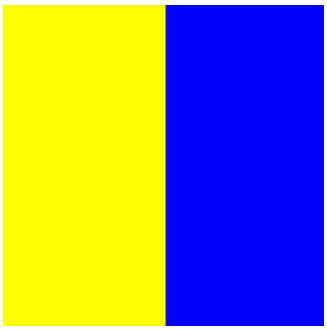

(c) Vertical split ($\theta = \frac{\pi}{2}$) without transition region.

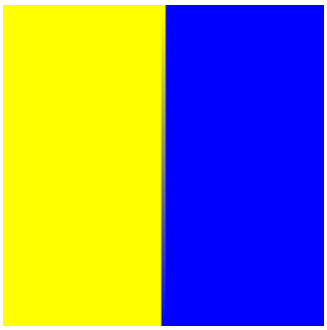

(d) Vertical split ($\theta = \frac{\pi}{2}$) with transition region.

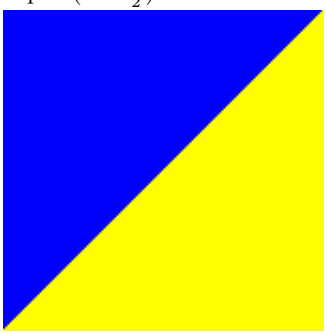

(e) Diagonal split from bottom left to top right ($\theta = \frac{\pi}{4}$) without transition region.

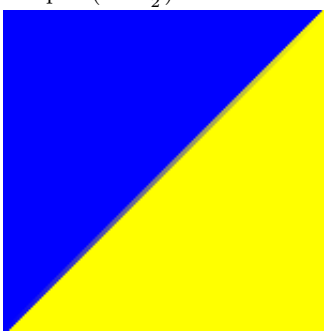

(f) Diagonal split from bottom left to top right ($\theta = \frac{\pi}{4}$) with transition region.

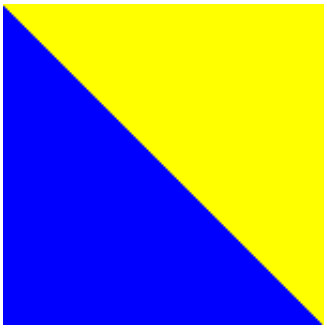

(g) Diagonal split from top left to bottom right ($\theta = \frac{3\pi}{4}$) without transition region.

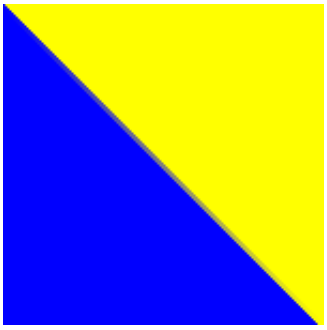

(h) Diagonal split from top left to bottom ($\theta = \frac{3\pi}{4}$) right with transition region.

Figure 30: Synthetic images created for color pair P_6.

7.2 Synthetic Segmentation Images

7.2.1 Manhattan Distance

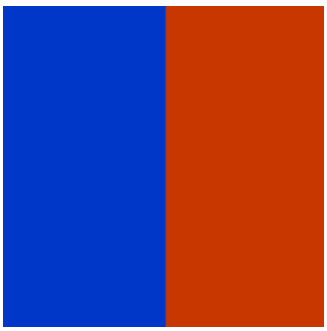

(a) Segmentation image for $\theta = \frac{\pi}{2}$ without transition region at $\alpha = 5228$.

(b) Segmentation image for $\theta = \frac{\pi}{2}$ with transition region at $\alpha = 2627$.

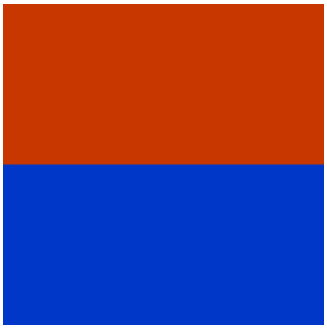

(c) Segmentation image for $\theta = 0$ without transition region at $\alpha = 5228$.

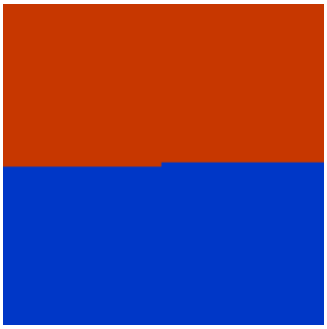

(d) Segmentation image for $\theta = 0$ without transition region at $\alpha = 2627$.

(e) Segmentation image for $\theta = \frac{\pi}{4}$ without transition region at $\alpha = 5228$.

(f) Segmentation image for $\theta = \frac{\pi}{4}$ with transition region at $\alpha = 104$.

(g) Segmentation image for $\theta = \frac{3\pi}{4}$ without transition region at $\alpha = 5228$.

(h) Segmentation image for $\theta = \frac{3\pi}{4}$ with transition region at $\alpha = 104$.

Figure 31: Segmentation images using D_{M} for the color pair P_1 with and without transition region.

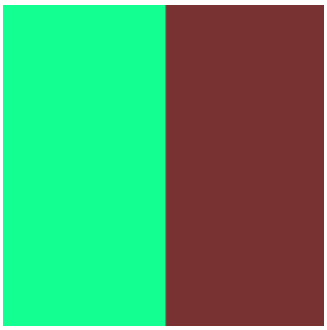

(a) Segmentation image for $\theta = \frac{\pi}{2}$ without transition region at $\alpha = 5228$.

(b) Segmentation image for $\theta = \frac{\pi}{2}$ with transition region at $\alpha = 2627$.

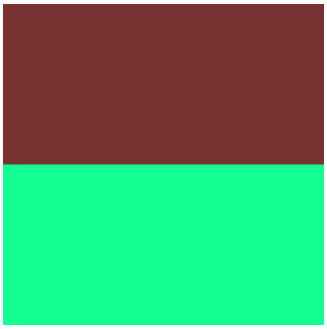

(c) Segmentation image for $\theta = 0$ without transition region at $\alpha = 5228$.

(d) Segmentation image for $\theta = 0$ without transition region at $\alpha = 2627$.

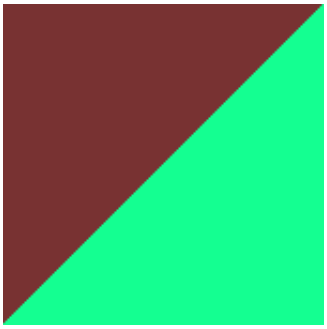

(e) Segmentation image for $\theta = \frac{\pi}{4}$ without transition region at $\alpha = 5228$.

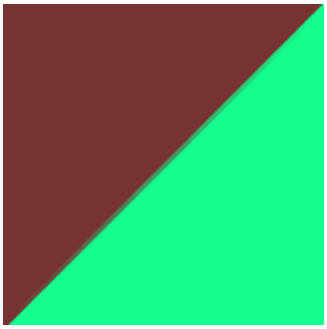

(f) Segmentation image for $\theta = \frac{\pi}{4}$ with transition region at $\alpha = 104$.

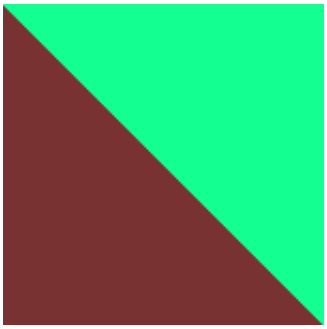

(g) Segmentation image for $\theta = \frac{3\pi}{4}$ without transition region at $\alpha = 5228$.

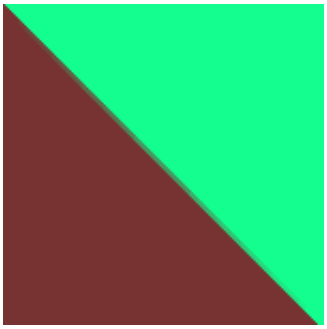

(h) Segmentation image for $\theta = \frac{3\pi}{4}$ with transition region at $\alpha = 104$.

Figure 32: Segmentation images using D_{M} for the color pair P_2 with and without transition region.

(a) Segmentation image for $\theta = \frac{\pi}{2}$ without transition region at $\alpha = 2261$.

(b) Segmentation image for $\theta = \frac{\pi}{2}$ with transition region at $\alpha = 1137$.

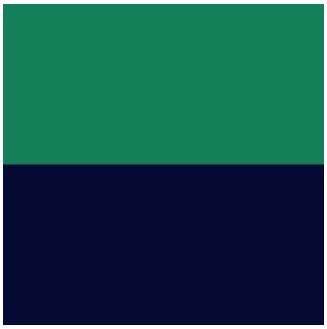

(c) Segmentation image for $\theta = 0$ without transition region at $\alpha = 2261$.

(d) Segmentation image for $\theta = 0$ without transition region at $\alpha = 1137$.

(e) Segmentation image for $\theta = \frac{\pi}{4}$ without transition region at $\alpha = 2261$.

(f) Segmentation image for $\theta = \frac{\pi}{4}$ with transition region at $\alpha = 78$.

(g) Segmentation image for $\theta = \frac{3\pi}{4}$ without transition region at $\alpha = 2261$.

(h) Segmentation image for $\theta = \frac{3\pi}{4}$ with transition region at $\alpha = 78$.

Figure 33: Segmentation images using D_{M} for the color pair P_3 with and without transition region.

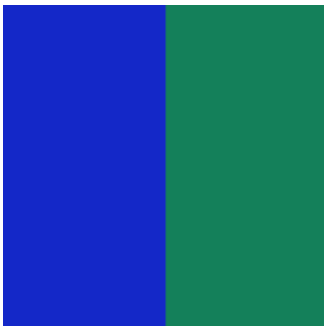

(a) Segmentation image for $\theta = \frac{\pi}{2}$ without transition region at $\alpha = 2588$.

(b) Segmentation image for $\theta = \frac{\pi}{2}$ with transition region at $\alpha = 1307$.

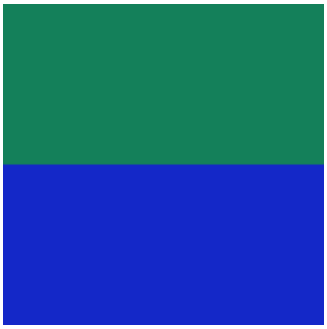

(c) Segmentation image for $\theta = 0$ without transition region at $\alpha = 2588$.

(d) Segmentation image for $\theta = 0$ without transition region at $\alpha = 1307$.

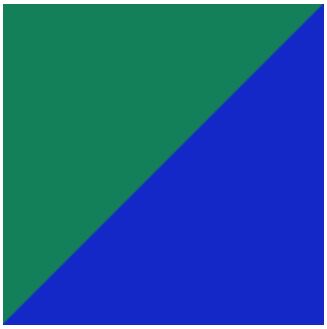

(e) Segmentation image for $\theta = \frac{\pi}{4}$ without transition region at $\alpha = 2588$.

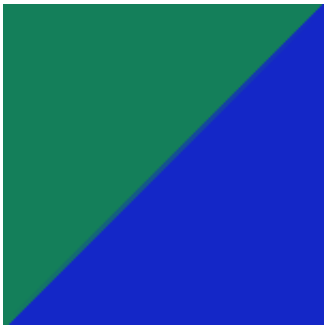

(f) Segmentation image for $\theta = \frac{\pi}{4}$ with transition region at $\alpha = 52$.

(g) Segmentation image for $\theta = \frac{3\pi}{4}$ without transition region at $\alpha = 2588$.

(h) Segmentation image for $\theta = \frac{3\pi}{4}$ with transition region at $\alpha = 52$.

Figure 34: Segmentation images using D_{M} for the color pair P_4 with and without transition region.

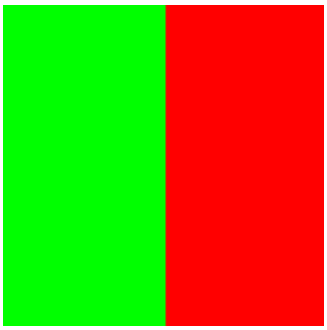

(a) Segmentation image for $\theta = \frac{\pi}{2}$ without transition region at $\alpha = 6666$.

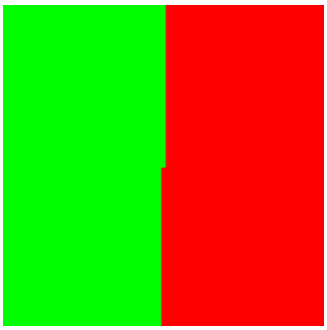

(b) Segmentation image for $\theta = \frac{\pi}{2}$ with transition region at $\alpha = 3359$.

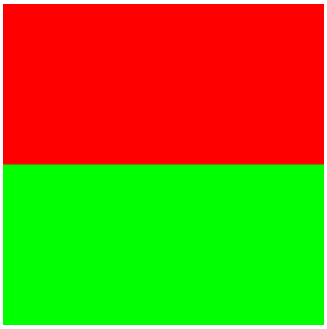

(c) Segmentation image for $\theta = 0$ without transition region at $\alpha = 6666$.

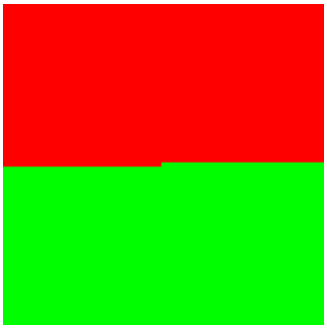

(d) Segmentation image for $\theta = 0$ without transition region at $\alpha = 3359$.

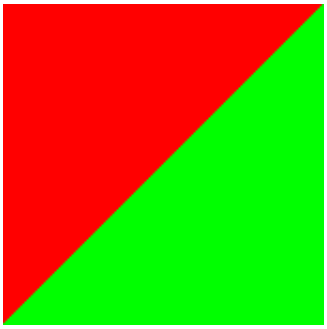

(e) Segmentation image for $\theta = \frac{\pi}{4}$ without transition region at $\alpha = 6666$.

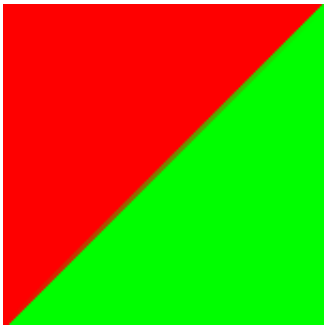

(f) Segmentation image for $\theta = \frac{\pi}{4}$ with transition region at $\alpha = 104$.

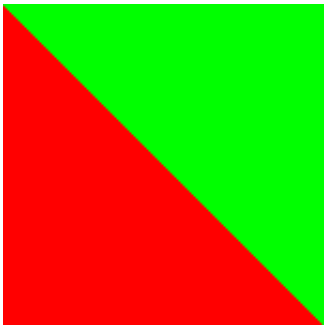

(g) Segmentation image for $\theta = \frac{3\pi}{4}$ without transition region at $\alpha = 6666$.

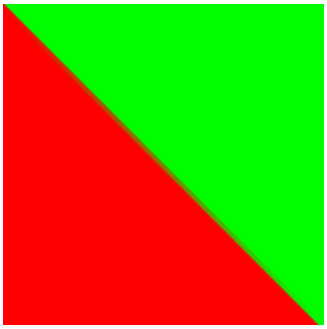

(h) Segmentation image for $\theta = \frac{3\pi}{4}$ with transition region at $\alpha = 104$.

Figure 35: Segmentation images using D_{M} for the color pair P_5 with and without transition region.

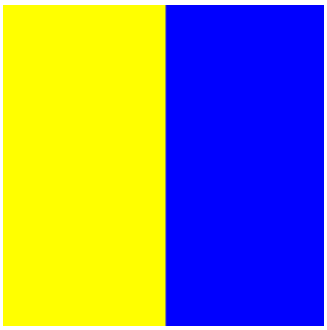

(a) Segmentation image for $\theta = \frac{\pi}{2}$ without transition region at $\alpha = 10000$.

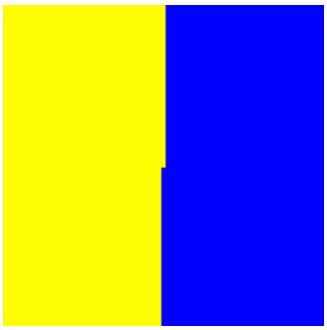

(b) Segmentation image for $\theta = \frac{\pi}{2}$ with transition region at $\alpha = 5032$.

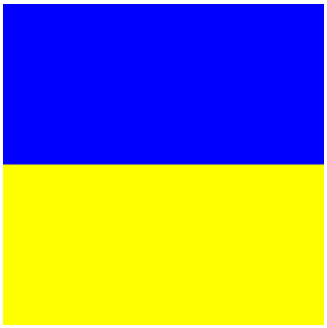

(c) Segmentation image for $\theta = 0$ without transition region at $\alpha = 10000$.

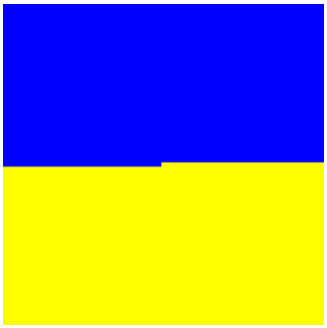

(d) Segmentation image for $\theta = 0$ without transition region at $\alpha = 5032$.

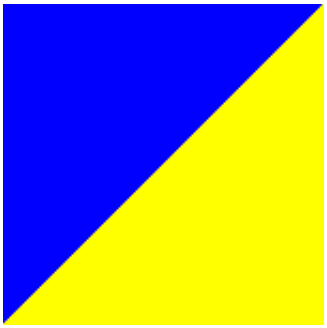

(e) Segmentation image for $\theta = \frac{\pi}{4}$ without transition region at $\alpha = 10000$.

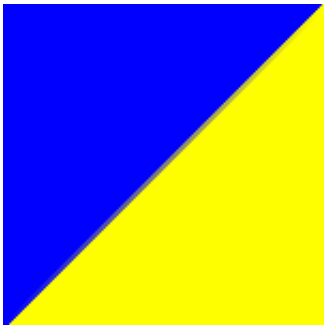

(f) Segmentation image for $\theta = \frac{\pi}{4}$ with transition region at $\alpha = 156$.

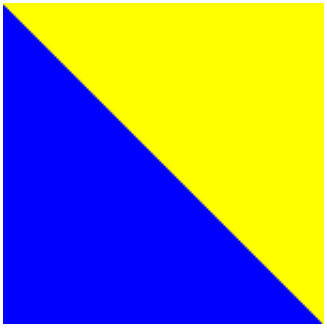

(g) Segmentation image for $\theta = \frac{3\pi}{4}$ without transition region at $\alpha = 10000$.

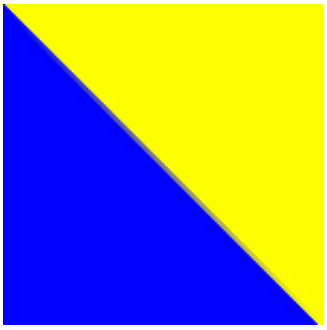

(h) Segmentation image for $\theta = \frac{3\pi}{4}$ with transition region at $\alpha = 156$.

Figure 36: Segmentation images using D_{M} for the color pair P_6 with and without transition region.

7.2.2 Euclidean Distance

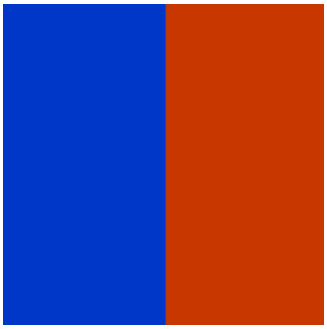

(a) Segmentation image for $\theta = \frac{\pi}{2}$ without transition region at $\alpha = 6403$.

(b) Segmentation image for $\theta = \frac{\pi}{2}$ with transition region at $\alpha = 3217$.

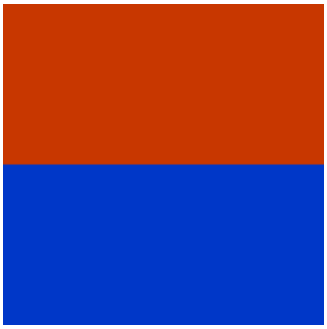

(c) Segmentation image for $\theta = 0$ without transition region at $\alpha = 6403$.

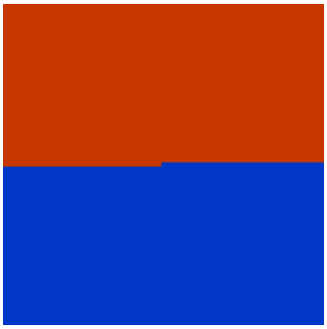

(d) Segmentation image for $\theta = 0$ without transition region at $\alpha = 3217$.

(e) Segmentation image for $\theta = \frac{\pi}{4}$ without transition region at $\alpha = 6403$.

(f) Segmentation image for $\theta = \frac{\pi}{4}$ with transition region at $\alpha = 128$.

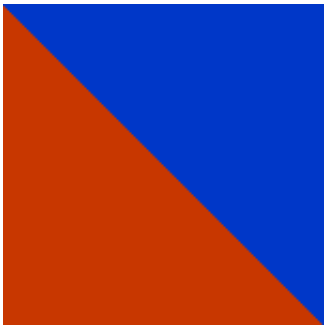

(g) Segmentation image for $\theta = \frac{3\pi}{4}$ without transition region at $\alpha = 6403$.

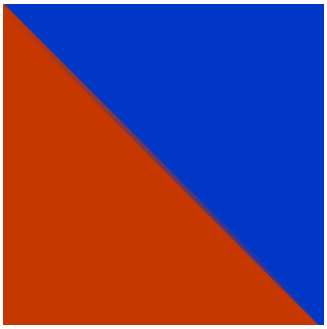

(h) Segmentation image for $\theta = \frac{3\pi}{4}$ with transition region at $\alpha = 128$.

Figure 37: Segmentation images using D_{E} for the color pair P_1 with and without transition region.

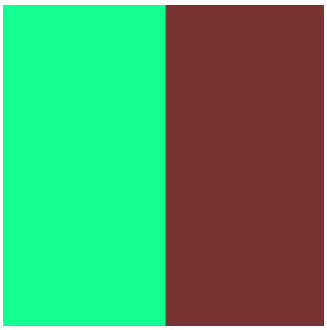

(a) Segmentation image for $\theta = \frac{\pi}{2}$ without transition region at $\alpha = 5594$.

(b) Segmentation image for $\theta = \frac{\pi}{2}$ with transition region at $\alpha = 2811$.

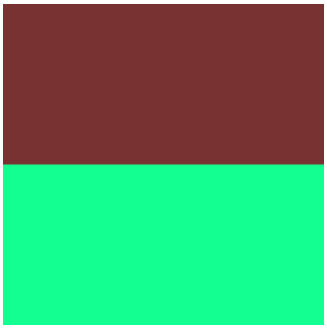

(c) Segmentation image for $\theta = 0$ without transition region at $\alpha = 5594$.

(d) Segmentation image for $\theta = 0$ without transition region at $\alpha = 2811$.

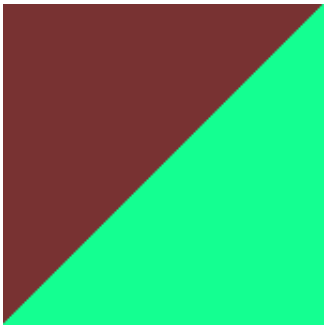

(e) Segmentation image for $\theta = \frac{\pi}{4}$ without transition region at $\alpha = 5594$.

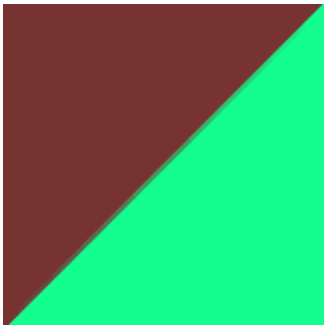

(f) Segmentation image for $\theta = \frac{\pi}{4}$ with transition region at $\alpha = 110$.

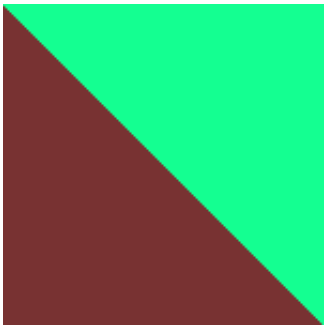

(g) Segmentation image for $\theta = \frac{3\pi}{4}$ without transition region at $\alpha = 5594$.

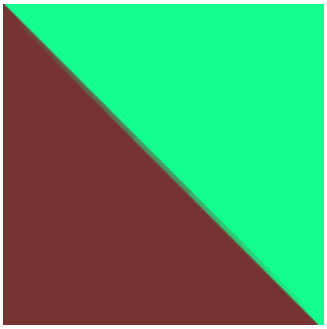

(h) Segmentation image for $\theta = \frac{3\pi}{4}$ with transition region at $\alpha = 110$.

Figure 38: Segmentation images using D_{E} for the color pair P_2 with and without transition region.

(a) Segmentation image for $\theta = \frac{\pi}{2}$ without transition region at $\alpha = 2841$.

(b) Segmentation image for $\theta = \frac{\pi}{2}$ with transition region at $\alpha = 1422$.

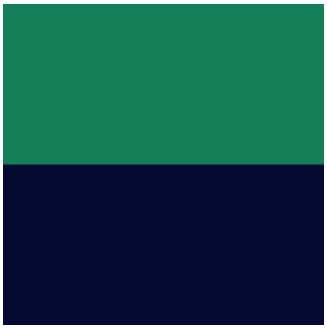

(c) Segmentation image for $\theta = 0$ without transition region at $\alpha = 2841$.

(d) Segmentation image for $\theta = 0$ without transition region at $\alpha = 1422$.

(e) Segmentation image for $\theta = \frac{\pi}{4}$ without transition region at $\alpha = 2841$.

(f) Segmentation image for $\theta = \frac{\pi}{4}$ with transition region at $\alpha = 78$.

(g) Segmentation image for $\theta = \frac{3\pi}{4}$ without transition region at $\alpha = 2841$.

(h) Segmentation image for $\theta = \frac{3\pi}{4}$ with transition region at $\alpha = 78$.

Figure 39: Segmentation images using D_{E} for the color pair P_3 with and without transition region.

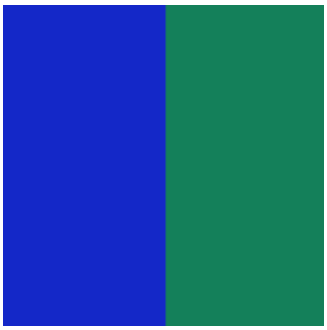

(a) Segmentation image for $\theta = \frac{\pi}{2}$ without transition region at $\alpha = 3189$.

(b) Segmentation image for $\theta = \frac{\pi}{2}$ with transition region at $\alpha = 1608$.

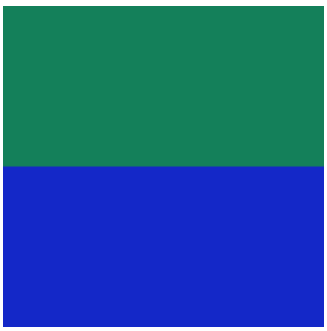

(c) Segmentation image for $\theta = 0$ without transition region at $\alpha = 3189$.

(d) Segmentation image for $\theta = 0$ without transition region at $\alpha = 1608$.

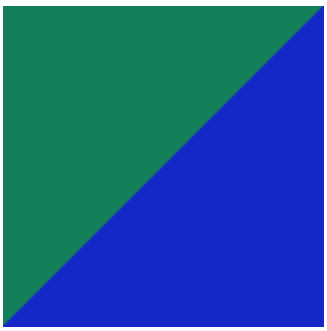

(e) Segmentation image for $\theta = \frac{\pi}{4}$ without transition region at $\alpha = 3189$.

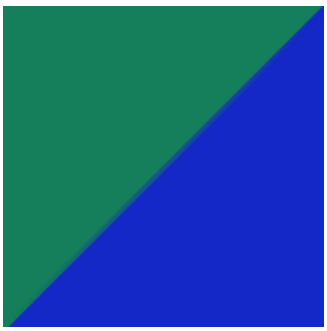

(f) Segmentation image for $\theta = \frac{\pi}{4}$ with transition region at $\alpha = 64$.

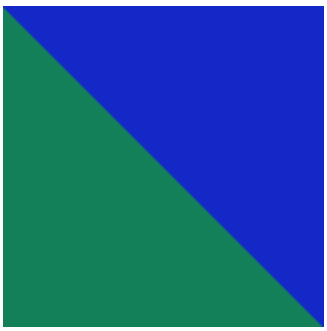

(g) Segmentation image for $\theta = \frac{3\pi}{4}$ without transition region at $\alpha = 3189$.

(h) Segmentation image for $\theta = \frac{3\pi}{4}$ with transition region at $\alpha = 64$.

Figure 40: Segmentation images using D_{E} for the color pair P_4 with and without transition region.

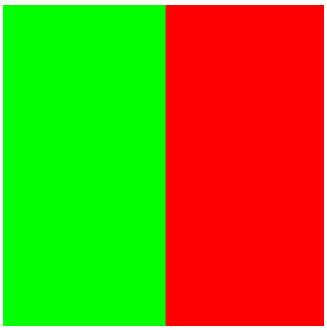

(a) Segmentation image for $\theta = \frac{\pi}{2}$ without transition region at $\alpha = 8164$.

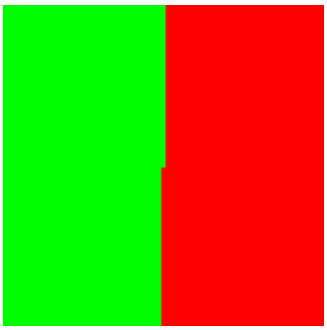

(b) Segmentation image for $\theta = \frac{\pi}{2}$ with transition region at $\alpha = 4114$.

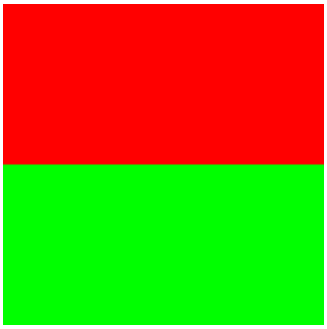

(c) Segmentation image for $\theta = 0$ without transition region at $\alpha = 8164$.

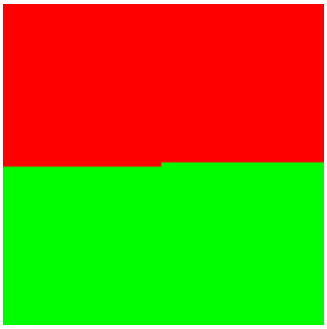

(d) Segmentation image for $\theta = 0$ without transition region at $\alpha = 4114$.

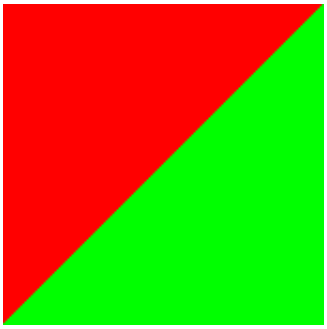

(e) Segmentation image for $\theta = \frac{\pi}{4}$ without transition region at $\alpha = 8164$.

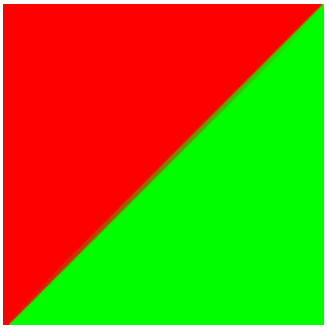

(f) Segmentation image for $\theta = \frac{\pi}{4}$ with transition region at $\alpha = 128$.

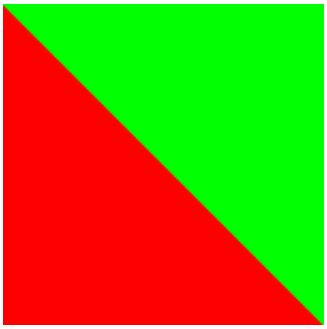

(g) Segmentation image for $\theta = \frac{3\pi}{4}$ without transition region at $\alpha = 8164$.

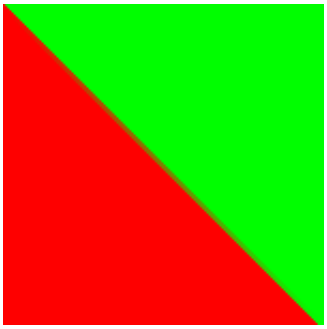

(h) Segmentation image for $\theta = \frac{3\pi}{4}$ with transition region at $\alpha = 128$.

Figure 41: Segmentation images using D_{E} for the color pair P_5 with and without transition region.

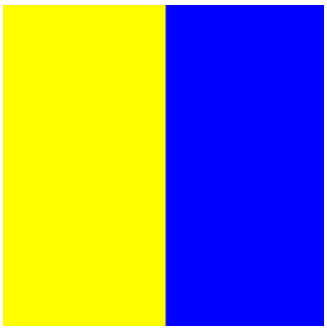

(a) Segmentation image for $\theta = \frac{\pi}{2}$ without transition region at $\alpha = 10000$.

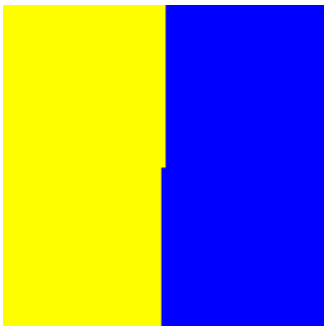

(b) Segmentation image for $\theta = \frac{\pi}{2}$ with transition region at $\alpha = 5032$.

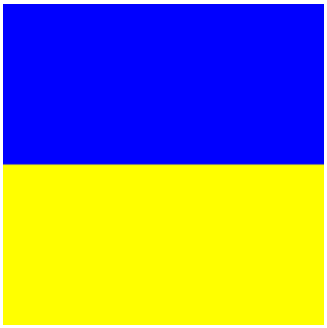

(c) Segmentation image for $\theta = 0$ without transition region at $\alpha = 10000$.

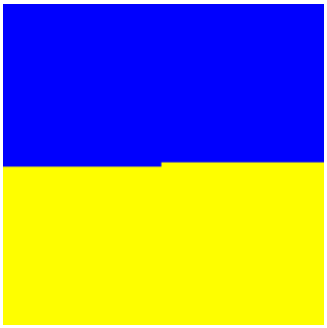

(d) Segmentation image for $\theta = 0$ without transition region at $\alpha = 5032$.

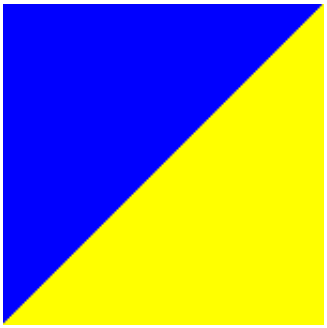

(e) Segmentation image for $\theta = \frac{\pi}{4}$ without transition region at $\alpha = 10000$.

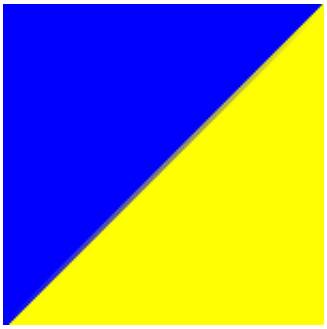

(f) Segmentation image for $\theta = \frac{\pi}{4}$ with transition region at $\alpha = 156$.

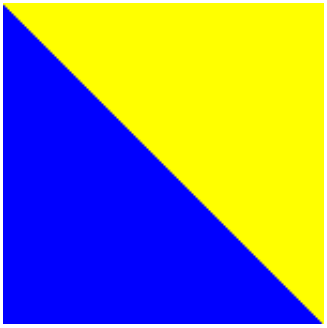

(g) Segmentation image for $\theta = \frac{3\pi}{4}$ without transition region at $\alpha = 10000$.

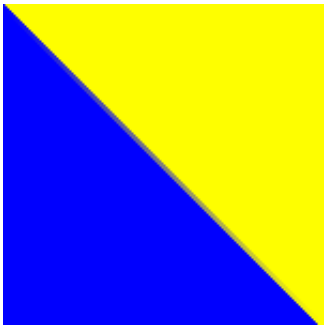

(h) Segmentation image for $\theta = \frac{3\pi}{4}$ with transition region at $\alpha = 156$.

Figure 42: Segmentation images using D_{E} for the color pair P_6 with and without transition region.

7.2.3 Cosine Distance

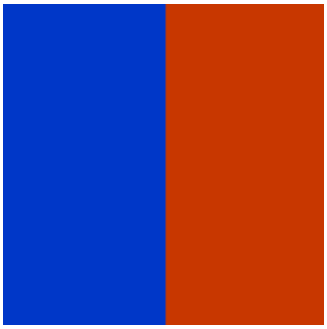

(a) Segmentation image for $\theta = \frac{\pi}{2}$ without transition region at $\alpha = 9296$.

(b) Segmentation image for $\theta = \frac{\pi}{2}$ with transition region at $\alpha = 2653$.

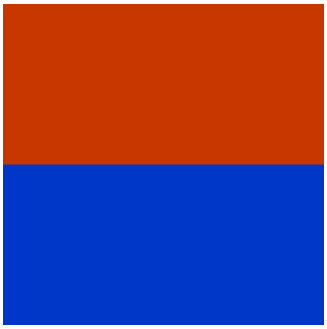

(c) Segmentation image for $\theta = 0$ without transition region at $\alpha = 9296$.

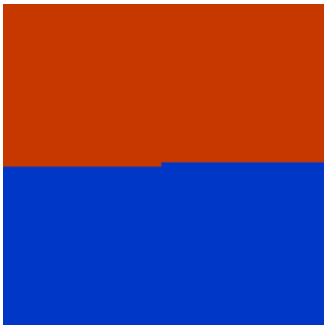

(d) Segmentation image for $\theta = 0$ without transition region at $\alpha = 2653$.

(e) Segmentation image for $\theta = \frac{\pi}{4}$ without transition region at $\alpha = 9296$.

(f) Segmentation image for $\theta = \frac{\pi}{4}$ with transition region at $\alpha = 3$.

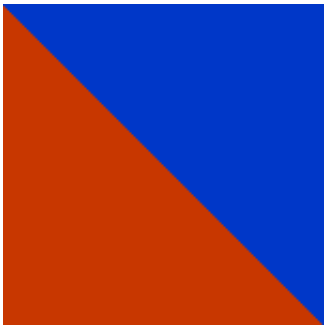

(g) Segmentation image for $\theta = \frac{3\pi}{4}$ without transition region at $\alpha = 9296$.

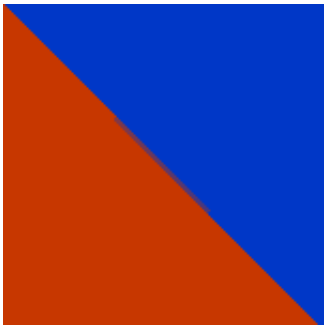

(h) Segmentation image for $\theta = \frac{3\pi}{4}$ with transition region at $\alpha = 3$.

Figure 43: Segmentation images using D_{C} for the color pair P_1 with and without transition region.

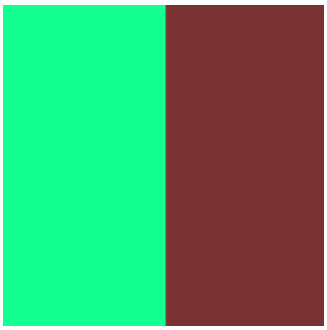

(a) Segmentation image for $\theta = \frac{\pi}{2}$ without transition region at $\alpha = 4530$.

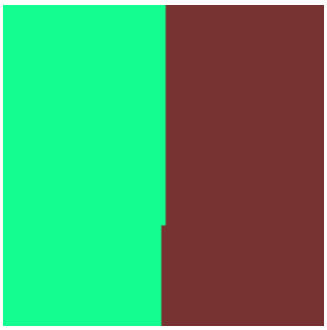

(b) Segmentation image for $\theta = \frac{\pi}{2}$ with transition region at $\alpha = 1167$.

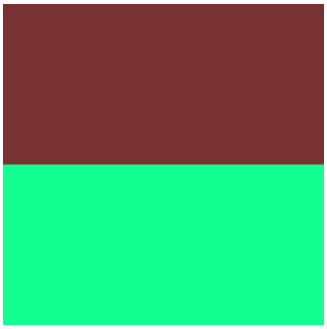

(c) Segmentation image for $\theta = 0$ without transition region at $\alpha = 4530$.

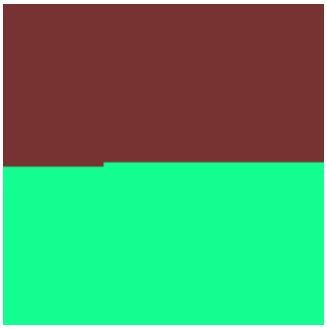

(d) Segmentation image for $\theta = 0$ without transition region at $\alpha = 1167$.

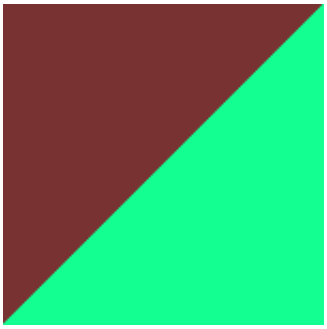

(e) Segmentation image for $\theta = \frac{\pi}{4}$ without transition region at $\alpha = 4530$.

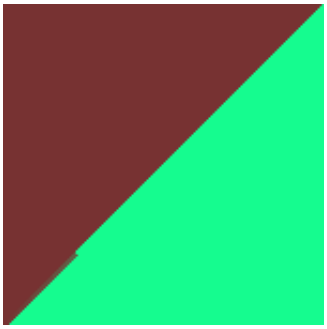

(f) Segmentation image for $\theta = \frac{\pi}{4}$ with transition region at $\alpha = 2$.

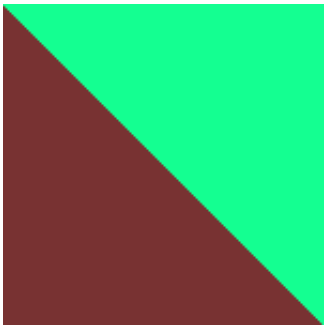

(g) Segmentation image for $\theta = \frac{3\pi}{4}$ without transition region at $\alpha = 4530$.

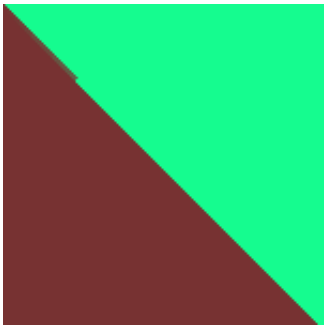

(h) Segmentation image for $\theta = \frac{3\pi}{4}$ with transition region at $\alpha = 2$.

Figure 44: Segmentation images using D_{C} for the color pair P_2 with and without transition region.

(a) Segmentation image for $\theta = \frac{\pi}{2}$ without transition region at $\alpha = 2724$.

(b) Segmentation image for $\theta = \frac{\pi}{2}$ with transition region at $\alpha = 682$.

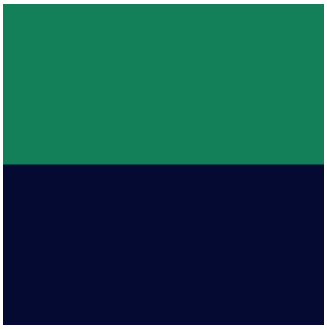

(c) Segmentation image for $\theta = 0$ without transition region at $\alpha = 2724$.

(d) Segmentation image for $\theta = 0$ without transition region at $\alpha = 682$.

(e) Segmentation image for $\theta = \frac{\pi}{4}$ without transition region at $\alpha = 2724$.

(f) Segmentation image for $\theta = \frac{\pi}{4}$ with transition region at $\alpha = 3$.

(g) Segmentation image for $\theta = \frac{3\pi}{4}$ without transition region at $\alpha = 2724$.

(h) Segmentation image for $\theta = \frac{3\pi}{4}$ with transition region at $\alpha = 3$.

Figure 45: Segmentation images using D_{C} for the color pair P_3 with and without transition region.

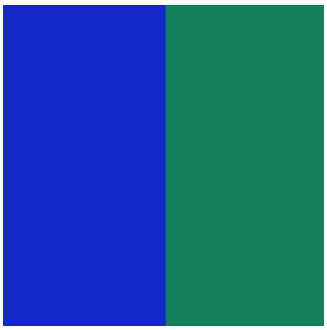

(a) Segmentation image for $\theta = \frac{\pi}{2}$ without transition region at $\alpha = 2724$.

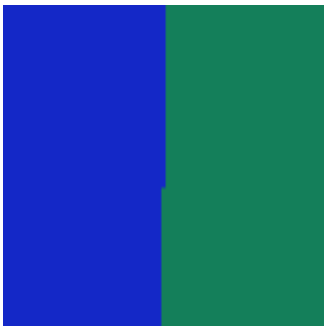

(b) Segmentation image for $\theta = \frac{\pi}{2}$ with transition region at $\alpha = 690$.

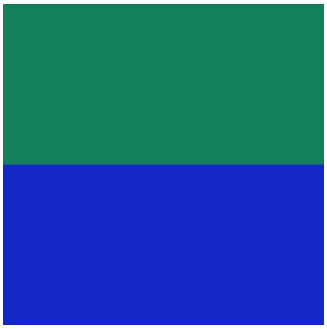

(c) Segmentation image for $\theta = 0$ without transition region at $\alpha = 2724$.

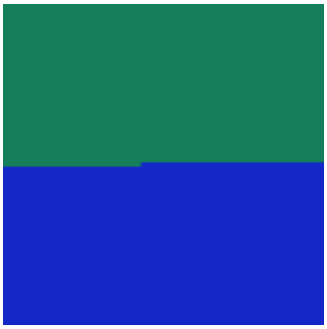

(d) Segmentation image for $\theta = 0$ without transition region at $\alpha = 690$.

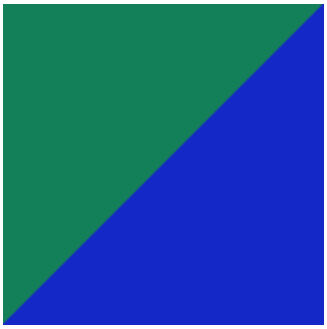

(e) Segmentation image for $\theta = \frac{\pi}{4}$ without transition region at $\alpha = 2724$.

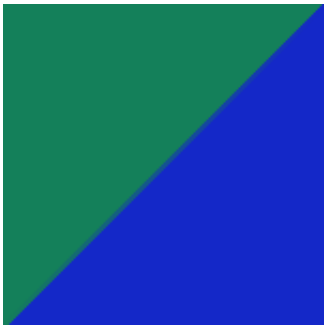

(f) Segmentation image for $\theta = \frac{\pi}{4}$ with transition region at $\alpha = 0$.

(g) Segmentation image for $\theta = \frac{3\pi}{4}$ without transition region at $\alpha = 2724$.

(h) Segmentation image for $\theta = \frac{3\pi}{4}$ with transition region at $\alpha = 0$.

Figure 46: Segmentation images using D_{C} for the color pair P_4 with and without transition region.

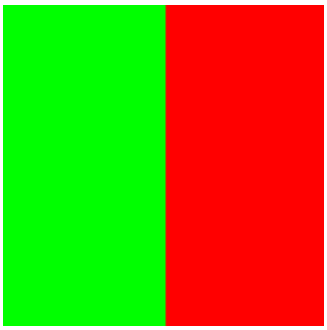

(a) Segmentation image for $\theta = \frac{\pi}{2}$ without transition region at $\alpha = 10000$.

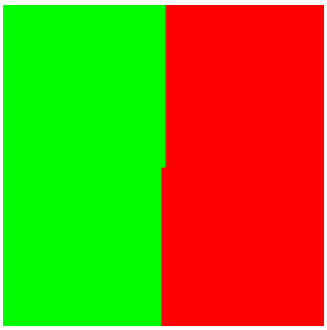

(b) Segmentation image for $\theta = \frac{\pi}{2}$ with transition region at $\alpha = 2874$.

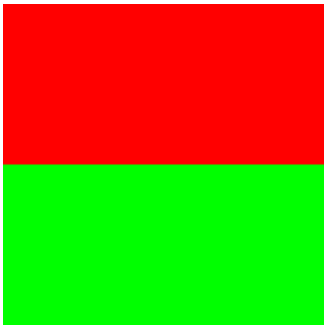

(c) Segmentation image for $\theta = 0$ without transition region at $\alpha = 10000$.

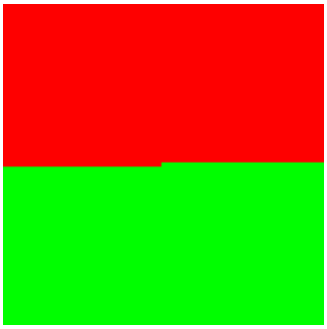

(d) Segmentation image for $\theta = 0$ without transition region at $\alpha = 2874$.

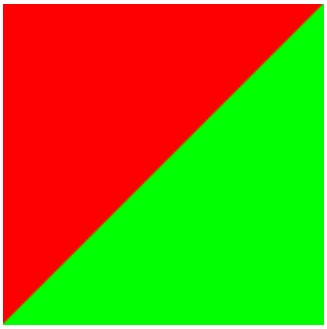

(e) Segmentation image for $\theta = \frac{\pi}{4}$ without transition region at $\alpha = 10000$.

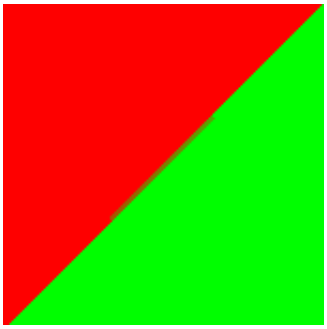

(f) Segmentation image for $\theta = \frac{\pi}{4}$ with transition region at $\alpha = 2$.

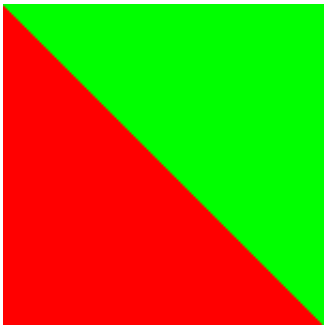

(g) Segmentation image for $\theta = \frac{3\pi}{4}$ without transition region at $\alpha = 10000$.

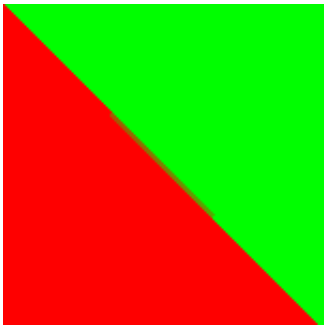

(h) Segmentation image for $\theta = \frac{3\pi}{4}$ with transition region at $\alpha = 2$.

Figure 47: Segmentation images using D_{C} for the color pair P_5 with and without transition region.

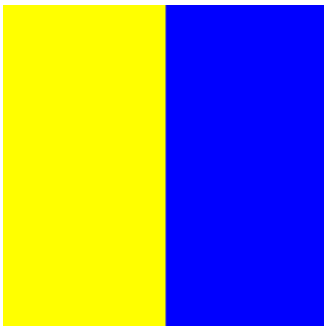

(a) Segmentation image for $\theta = \frac{\pi}{2}$ without transition region at $\alpha = 10000$.

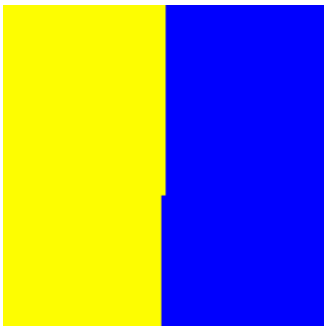

(b) Segmentation image for $\theta = \frac{\pi}{2}$ with transition region at $\alpha = 2861$.

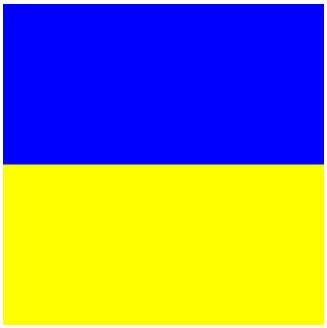

(c) Segmentation image for $\theta = 0$ without transition region at $\alpha = 10000$.

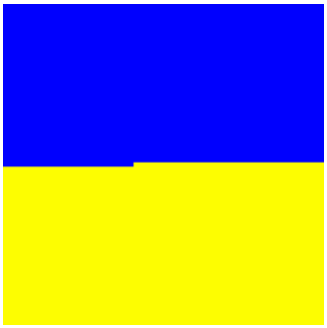

(d) Segmentation image for $\theta = 0$ without transition region at $\alpha = 2861$.

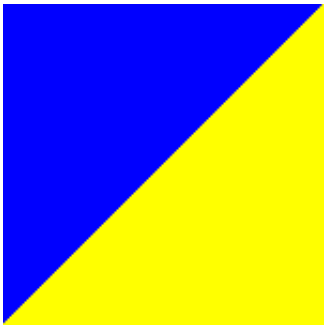

(e) Segmentation image for $\theta = \frac{\pi}{4}$ without transition region at $\alpha = 10000$.

(f) Segmentation image for $\theta = \frac{\pi}{4}$ with transition region at $\alpha = 2$.

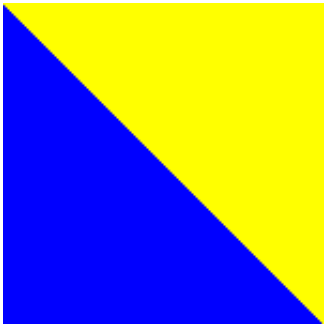

(g) Segmentation image for $\theta = \frac{3\pi}{4}$ without transition region at $\alpha = 10000$.

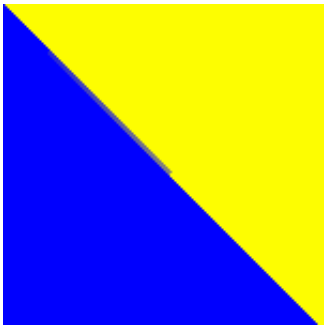

(h) Segmentation image for $\theta = \frac{3\pi}{4}$ with transition region at $\alpha = 2$.

Figure 48: Segmentation images using D_{C} for the color pair P_6 with and without transition region.